# Gli3 loss-of-function compromises vomeronasal neurogenesis, formation of olfactory ensheathing cells in the nasal mucosa, and GnRH-1 neuronal migration

Ed Zandro M. Taroc[1], Ankana Naik[1], Jennifer M Lin[1], Nicolas B Peterson[1], David Keefe[2], Elizabet Genis[1], Gabriele Fuchs[1], Ravikumar Balasubramanian[2], and Paolo E. Forni[1]**.**

[1]Department of Biological Sciences, University at Albany, State University of New York, Albany, NY 12222, USA.

[2] Harvard Reproductive Sciences Center and The Reproductive Endocrine Unit of the Department of Medicine, Massachusetts General Hospital, Boston, MA 02114, USA.

*Author for correspondence (pforni@albany.edu)

## Abstract

Gonadotropin-releasing-hormone-1 neurons (GnRH-1ns) control pubertal onset, and fertility. During mammalian development, GnRH-1ns migrate from the developing vomeronasal organ (VNO) into the brain, where they control the pituitary release of gonadotropins. Loss-of-function of the transcription factor Gli3 disrupts olfactory development, however, if Gli3 plays roles in GnRH-1 neuronal development is unclear. By analyzing Gli3 extra-toe mutants (Gli3$^{Xt/Xt}$), we found neurogenic defects in the VNO, lack of olfactory ensheathing cells in the nasal mucosa and disrupted GnRH-1 neuronal migration. We discovered that Gli3 loss-of-function impairs the formation of achaete-scute family bHLH transcription factor 1 (Ascl-1) positive vomeronasal progenitors, but not the onset of GnRH-1ns. Moreover, the dysmorphic brain of Gli3$^{Xt/Xt}$ mutants also displayed altered Semaphorin-3A expression, a key guidance cue for GnRH-1 migration. In contrast to Gli3$^{Xt/Xt}$, Ascl-1$^{null}$ mutants showed reduced neurogenesis for both vomeronasal and GnRH-1ns. The non-overlapping phenotype between Gli3$^{Xt/Xt}$ and Ascl-1$^{null}$ mutants suggests that Ascl-1 is crucial for GnRH-1 progenitors but, in these cells, independent of Gli3 control. Since Kallmann syndrome (KS) shows defects in GnRH migration, we examined KS patient samples using whole exome sequencing. We identified and validated a new *GLI3* loss-of-function variant. Our data suggest that *GLI3* is a candidate modifier gene contributing to KS etiology.

## Introduction

During embryonic development, the olfactory placode gives rise to multiple cell types, including migratory/pioneer neurons, terminal nerve cells, gonadotropin releasing hormone-1 (GnRH-1) neurons (GnRH-1ns), and the olfactory and vomeronasal sensory neurons (1, 2). GnRH-1ns migrate in close association with olfactory ensheathing cells (OECs) (3, 4) along the terminal nerve (2, 5, 6) from the vomeronasal organ into the hypothalamus, where they control gonadotropin release from the pituitary gland (7, 8). Though vomeronasal sensory neurons (VSNs) have not been identified in humans, the existence of a vomeronasal structure and migratory GnRH-1ns do exist during human embryonic development (2). These data suggest this structure can give rise to migratory neurons and terminal nerve fibers in humans (2). GnRH-1ns play a central role in controlling the reproductive axis of vertebrates. Defective development of the olfactory placode, impaired development of its derivatives, or defects in GnRH-1ns migration lead to Kallmann syndrome (KS), a rare human genetic disorder characterized by pubertal failure due to congenital hypogonadotropic hypogonadism (HH) and anosmia (impaired sense of smell) (9).

KS is phenotypically and genetically heterogeneous, which is inherited as X-linked recessive, autosomal recessive, or autosomal dominant. In the last three decades, various causal genes for KS have been identified including: anosmin-1 (*ANOS1*), fibroblast growth factor receptor 1 (*FGFR1*), fibroblast grow factor 8 (FGF8), Prokineticin Receptor 2 (*PROKR2*), Prokineticin 2 (*PROK2*), Chromodomain-helicase-DNA-binding protein 7 (*CHD7*), WD repeat-containing protein 11 (*WDR11*), Heparan Sulfate 6-O-Sulfotransferase 1 (*HS6ST1*), Semaphorin 3A (*SEMA3A*), Semaphorin 3E (*SEMA3E*), Interleukin 17 Receptor D (*IL17RD*), SRY [sex determining region Y]-box 10 (*SOX10*), and FEZ Family Zinc Finger 1 (*FEZF1*) (3, 10). Normosmic idiopathic hypogonadotropic hypogonadism [nIHH] represents another phenotypic form of HH, which is associated with a normal sense of smell and expression of several genes governing GnRH secretion/action in patients. Several KS individuals with pathogenic mutations display variable phenotypic penetrance/expressivity, which is only partially explained by allelic variability. A subset of KS patients also harbor mutations in 2 or more genes linked to either KS or nIHH (11-14), suggesting a oligogenic/multigenic etiology. However, the genetic basis for over half of KS phenotypes remains unknown.

Sonic hedgehog (Shh) is a key signaling factor essential for CNS and craniofacial and limb development (15-17). Gli3, together with Gli1 and Gli2, is under transcriptional regulation of sonic hedgehog (Shh) signaling. In the absence of Shh signaling, Gli3 and Gli2 act as transcriptional repressors. However, in the presence of active Shh signaling, Gli2 and Gli3 can function as transcriptional activators (18, 19). Once activated, Gli2 and Gli3 induce Gli1 expression, which may function as a transcriptional amplifier. Studies in animal models show that Gli3 loss-of-function can induce a spectrum of craniofacial defects, such as short nose with flat nasal bridge and cleft palate (20) and impaired development of the dorsal telencephalon that produces an expansion of ventral telencephalic and diencephalic regions (21-25). Consistent with these observations, *GLI3* mutations in humans can cause non-syndromic forms of polydactyly and syndromic forms of polydactyly like (a) Greig cephalopolysyndactyly syndrome [GCPS] (polydactyly and craniofacial anomalies) and (b) Pallister Hall Syndrome [PHS] (polydactyly, hypothalamic hamartoma, laryngeal cleft) (26).

Multiple lines of evidence from animal and human studies suggest that Gli3 function is critical for olfactory and GnRH neuronal development. While lack of functional Gli1 and Gli2 do not directly affect GnRH-1 neurogenesis and migration to the hypothalamus (27), the Gli3$^{pdn/pdn}$, a Gli3 hypomorphic mouse model lacking rostral olfactory bulb protrusions, show a delayed, but not missing, GnRH-1 neuronal migration (22, 24, 25). Gli3 loss-of-function mouse mutants termed Gli3 extra-toe (Gli3$^{Xt/Xt}$) show a severely disrupted olfactory system with a lack of olfactory bulb protrusions and the formation of ectopic olfactory bulb primordia (28-30). Some *GLI3* mutation positive GCPS and PHS human patients also display micropenis and undescended testes (26), two features suggesting HH. Craniofacial midline defects are also common in KS individuals (31).

Taken together, *GLI3* represents a compelling candidate gene for human KS/HH. A recent report identified 2 missense variants in the *GLI3* gene associated with HH subjects, suggesting a possible causal role for GLI3 in human hypogonadotropism (32). However, these human genetic findings do not present any mechanistic or functional roles for Gli3 in GnRH neuronal ontogeny. Genetic interactions between Gli3 and known HH candidate genes, such as FGF8(33), Sox10(34), CHD7(35) and WDR11 (36), suggest that Gli3 may function as a HH candidate modifier gene contributing to the oligogenic nature of KS/nIHH.

## RESULTS

### *Gli3 is expressed by apical progenitor cells that lead to VNO neuroprogenitor cells.*

Gli3 has been shown to be dispensable for olfactory sensory neuron (OSN) generation and maturation, but necessary for proper axonal routing which may be linked to GnRH-1 neuron development (29). GnRH-1ns are born in the nasal pit which eventually develops into the vomeronasal organ, so we analyzed Gli3 expression throughout GnRH-1 and VSN development. GnRH-1ns were immunodectable at E11.5, before any vomeronasal neuron formation (Fig.1A,A1,M,P) (5, 9, 37, 38). By E13.5 – E15.5, we observed that the developing VNO was populated by Tfap2e (AP-2ε) and Meis2 positive VSNs (Fig.1N,Q), however, most of the GnRH-1ns have migrated out of the vomeronasal area by E13.5 (Fig.1B,B1,C,C1).

We performed in-situ hybridization and immunohistochemistry (Data not shown) against Gli3 at embryonic stages (E) E11.5, E13.5, and E15.5 (Fig.1D-F). These experiments revealed that Gli3 mRNA and protein localize in the apical regions of the developing vomeronasal epithelia. The apical cells in the developing olfactory pit have been shown to be Hes-1 positive proliferative stem cell/progenitors that give rise, over time, to apical Ascl-1 neurogenic progenitors (39). To study this further in the developing VNO we performed immunostaining using phospho-Histone-H3 (PHH3), where we detected mitotic cells only in the apical region of the VNO at E11.5, but by E13.5 and E15.5 we detected mitotic cells along the margins of both apical and basal regions (39, 40) (Fig.1G-I). Immunostaining for Hes-1 and Ascl-1 in the developing VNO (Fig.2A-D) was consistent with these findings. We also observed that very few Ascl-1 positive cells at E11.5 but remained in the basal portions of the developing vomeronasal epithelium at E13.5 and E15.5 (Fig.1J-L). These data suggest that GnRH-1 and VSN neurogenesis occur at distinct developmental stages.

A detailed analysis at E15.5 confirmed the opposite expression pattern for Hes-1 and Ascl-1, as Hes-1 localized to the apical portions and Ascl-1 in the in the basal portions of the VNO (Fig.2A,D). We confirmed Gli3 immunoreactivity in Hes-1 positive cells and sparse immunoreactivity in the basal regions of the VNO. The immunoreactivity of Gli3 in the proliferative apical regions of the VNO prompted us to analyze if Gli3 repressor activity contributes to initiating the differentiation of neurogenic progenitors (17, 41).

## Gli3 loss-of-function affects VSNs neurogenesis but is compatible with VSN specification and differentiation.

The expression pattern of Gli3 in apical region of the VNO resembles its expression in the ventricular zone of the developing brain cortex (17). We speculated that Gli3 may play a similar role as in the cortex, aiding in stimulating the onset of neurogenic progenitors responsible for the genesis of GnRH-1ns, terminal nerve cells, and VSNs. VSNs can differentiate into either apical or basal VSNs (42). To identify and quantify the cell bodies of the embryonic VSNs, we performed immunolabeling on Gli3$^{Xt/Xt}$ mutants and controls against the transcription factors Meis2 and Tfap2e (AP-2$\varepsilon$) (43, 44) (Fig.3 A,B). At E15, we detected both apical and basal VSNs in the developing VNOs of controls (Fig.3A). However, we found a dramatic reduction (~70%) in the number of VSNs in Gli3$^{Xt/Xt}$ null mutants. (Fig.3C). Heterozygous Gli3$^{WT/Xt}$ displayed an intermediate phenotype between controls and Gli3$^{Xt/Xt}$ mutants. These data suggest that lacking functional Gli3 compromises VSNs neurogenesis, but the few generated neurons can differentiate into the two main types of VSNs (Fig.3A-C).

Quantifications of PHH3+ mitotic cells at E15 highlighted a significant decrease in the total number of mitotic progenitors in Gli3$^{Xt/Xt}$ mutants (Fig.3E,F,D). However, we found a significant reduction in the number of basal progenitors in Gli3$^{Xt/Xt}$ compared to WT animals and found no significant difference in apical cells (Fig.3D). Heterozygous Gli3$^{WT/Xt}$ embryos displayed an intermediate, non-significant difference compared to WT or Gli3$^{Xt/Xt}$. Since we found a significant reduction in proliferation in the basal portions of the VNO, we verified if Gli3 loss-of-function compromised the onset of Ascl-1 positive basal neurogenic progenitors. Quantifications of Ascl-1 positive cells confirmed a dramatic (~90%) reduction of Ascl-1+ neurogenic progenitors (Fig.3H,I,E). These data suggest that Gli3 loss-of-function in the VNO impairs the onset of neurogenic progenitors, similarly to what was recently described in the developing brain cortex (17, 41). We conclude that the loss of Gli3 mediated gene repression negatively affects the onset of neurogenic progenitors in the VNO.

## Gli3 loss disrupts terminal nerve routing and GnRH-1 neuronal migration

Since we observed defects in VSN development, we investigated the impact of Gli3 loss-of-function on GnRH-1 neurogenesis and migration. In control conditions, GnRH-1ns migrate along the axons of the terminal nerve that invades the brain ventral to the olfactory bulb, crosses the developing ventral telencephalon/sub-pallium and then projects to the preoptic area (5, 45-47) (Fig.4A,C,D,G). However, in Gli3$^{Xt/Xt}$ mutants, most GnRH-1ns were unable to reach the brain, and instead formed large clusters of cells in the nasal area (Fig.4B,E). In Gli3$^{Xt/Xt}$ mutants, some GnRH-1ns migrated toward the developing brain but then formed cell clumps along the migratory track (Fig.4F). A sparse number of GnRH-1ns did reach the putative forebrain junction without invading the brain, but extended their axons around the dorsal-most portions of the brain (Fig.4B,H).

We then quantified the distribution of GnRH-1ns between the nasal area forebrain junction and brain on serial parasagittal sections immuno-stained against GnRH-1 (Fig.4I). These data revealed a lack of GnRH-1 immunoreactive cells in the brain of Gli3 mutants with a massive accumulation of GnRH-1 cells in the nasal area. We observed a small, but significant, reduction in the number of GnRH-1 positive cells in the brain of heterozygous controls at E15.5 with a comparable increase in GnRH-1 cells in the nasal area. Notably, quantifications on WT, Gli3$^{Xt/WT}$, and Gli3$^{Xt/Xt}$ mutants at E15.5 revealed that the total number of GnRH-1ns was comparable across genotypes, in contrast with what we observed for VSNs. These data indicate that Gli3 loss-of-function, which compromises the formation of Ascl-1 positive vomeronasal progenitors (Fig.3), disrupts normal GnRH-1 neuronal migration but does not prevent GnRH-1 neurogenesis or differentiation.

## Gli3 null mutants display misrouting of the vomeronasal nerve without OEC.

To understand if the defective migration of GnRH-1ns in Gli3$^{Xt/Xt}$ results from defective vomeronasal development and/or aberrant terminal nerve projections to the brain, we performed a series of immunolabeling experiments to discriminate between cell types. Immunolabeling with anti-peripherin provided a shared marker to highlight olfactory, vomeronasal, and terminal nerve neurons (Fig.5A-D,M,N)(5). To follow the projections of VSNs and the terminal nerve (See cartoon in Fig.5; Fig.5A-D), we performed immunolabeling against the guidance receptors, Neuropilin-2 (Nrp2), Roundabout-2 (Robo2) and Neuropilin-1 (Nrp1). Robo2 highlights the projections of the basal VSNs (Fig.5E,F,I,J), Nrp2 highlights apical VSNs (Fig.5G-J) (48), while Nrp1 (Fig.5K2,L2)(5) labels the projections of putative terminal nerve neurons (Fig.5K1-L2). In control animals, we found the TN fibers (Nrp1+) invaded the brain, together with GnRH-1ns (Fig.5A,C,E,G,I). However, Gli3$^{Xt/Xt}$ mutants showed stalled olfactory and vomeronasal axons (positive for Robo2 and/or Nrp2, Fig.5B,D,F,H,J) (29) in front of the forebrain, which formed a FCM. However, we did observe that sparse putative terminal nerve axons and GnRH-1ns (Fig.5B,L1,L2) reached the putative forebrain junction and projected around the dorsal portions of the brain. However, the majority of GnRH-1ns (Fig.4E) and terminal nerve fibers (Peripherin+;Nrp1+ see Fig.5 O1-O4; negative for Nrp2 and Robo2, Fig.5N-N4) formed large tangles in the nasal area. These data show that Gli3 loss-of-function leads to defective vomeronasal and terminal nerve trajectories, which phenocopies a loss of OECs in Sox10 null mouse mutants (3, 4).

To test the possible implication of OECs in axonal misrouting and GnRH-1 migratory defects that we observed in Gli3$^{Xt/Xt}$ mutants, we performed double staining against Peripherin and Sox10(3, 49, 50). In control animals, Sox10 positive OECs were localized proximal to the basal lamina of the vomeronasal epithelium and were associated with the vomeronasal bundles emerging from the vomeronasal epithelium (Fig.5P,R). In the OE and olfactory fibers, we observed a similar distribution with strong Sox10 immunoreactivity close to the basal regions of the OE and along the olfactory bundles projecting to the OBs (Fig.5P). In Gli3$^{Xt/Xt}$ mutants, we found a nearly complete lack of Sox10 immunoreactivity around the vomeronasal epithelium, and no Sox10+ cells associated with vomeronasal axons or terminal nerve (Fig.5Q,S). We also found no Sox10 immunoreactivity near the basal lamina of the olfactory epithelium (Fig.5Q).

However, as previously described by others (29), in Gli3$^{Xt/Xt}$ we found Sox10 positive ensheathing cells proximal to the brain as part of the FCM (29), (Fig.5Q).

As we detected dramatic defects in OECs formation in the developing olfactory system, we propose that the aberrant neuronal patterning and GnRH-1 migratory impairment observed in Gli3$^{Xt/Xt}$ mutants must, at least in part, be secondary to the lack of OECs in the nasal mucosa (3, 4, 50).

## Delayed not defective migration in Gli3$^{Xt/WT}$ heterozygous mutants

Partial defects in GnRH-1 neuronal migration in Gli3$^{Pdn/Pdn}$ Gli3 hypomorphs (51) suggest that defects in Gli3 levels can impair GnRH-1 neuronal migration. As we collected evidence pointing to a role for Gli3 in controlling neurogenesis of the VSNs, we further analyzed the development of the GnRH-1 system in Gli3$^{Xt/WT}$ heterozygous embryos. Gli3$^{Xt/WT}$ are viable, fertile, have mild craniofacial defects and an extra toe (52) but do not display obvious abnormalities in the olfactory system. We analyzed GnRH-1 neuronal migration in Gli3$^{Xt/WT}$ heterozygous animals after completing development. Analysis of adult WT controls and Gli3$^{Xt/WT}$ mutants (Fig.7A-C) revealed no significant differences in number and distribution of GnRH-1ns in the brain after completing development. Immunostaining against GnRH-1 and quantifying the average area of GnRH-1 immunoreactive axons also revealed comparable GnRH-1 innervation of the median eminence (Fig.6D-F). These data suggest that Gli3 haploinsufficiency mice show delayed, but not disrupted, GnRH-1 neuronal migration.

## Gli3$^{Xt/Xt}$ mutants show dysmorphic brain development and altered Sema3A expression

Since brain development can be highly dysmorphic after Gli3 loss-of-function (17, 25, 29, 52-54), we analyzed how aberrant development of the forebrain could indirectly compromise GnRH-1 neuronal migration. In rodents, gamma-aminobutyric acid (GABA)-ergic interneurons form in the ventral telencephalon and subsequently migrate toward the cortex (55-59). The transcription factor AP-2ε can identify the developing olfactory bulbs and vomeronasal neurons (30, 43, 60) (Fig.7A-D). We used antibodies against the glutamate decarboxylase 1 (brain, 67kDa) (GAD67/GAD-1) to label the ventral forebrain/subpallium. Consistent with previous reports (23, 30), Gli3$^{Xt/Xt}$ mutants exhibit a lack of rostral olfactory bulb protrusions but the formation of ectopic olfactory bulb-like structures, positive for AP-2$\varepsilon$ (30), in the dorsal/lateral portions of the developing telencephalon (Fig.7B ,D) . At E15.5, GnRH-1ns invade the brain by crossing the putative accumbens (ventral to the OB) and then steering ventrally towards the hypothalamic area.

During embryonic development Sema3A is expressed ventral to the OB in the putative accumbens/ “septostriatal transition area” (Fig.7E,G). Lack of Sema3A is not compatible with normal invasion of the brain by the GnRH-1ns (45). As the development of the brain appears highly dysmorphic in Gli3 mutants (See cartoon in 7F), we analyzed the pattern of Sema3A expression compared to controls. Our analysis revealed that Gli3$^{Xt/Xt}$ mutants showed comparable Sema3A expression to controls in nasal areas and in the hindbrain. However, we found a near complete absence of Sema3A expression in the expanded subpallium and in the dorsal portion of the forebrain (Fig.7B,D). These data suggest that Gli3 loss-of-function compromises Sema3A expression and patterning in the brain which, alone, is a molecular condition sufficient to alter GnRH-1 migration (45).

## Loss of Ascl-1 disrupts normal VNO and GnRH-1ns development

The negative effects of Gli3 loss-of-function on VSNs but not on GnRH-1 neurogenesis prompted us experimentally test 1) if GnRH-1 neurogenesis depends on the transcriptional activity of Ascl-1 (61) and 2) if the migratory phenotype observed in Gli3 mutants and the lack of OECs in the mucosa directly reflects the compromised neurogenesis in the OE and VNO. We analyzed GnRH-1, VSN, and OECs development in Ascl-1 KO mutants at E13.5. At this developmental stage the TN and VSNs form Peripherin positive bundles of fibers projecting towards the brain. In control animals, we observed GnRH-1ns emerging from the VNO and migrating towards the brain (Fig.8A,C). As reported, analysis of Ascl-1 KOs showed a dramatic (~62%) reduction in the number of VSNs and a reduction in Peripherin positive axonal projections emerging from the developing VNO (Fig.8A,C,E,G,O). However, GnRH-1 immunoreactive neurons, like controls, emerged from the developing VNO and migrated toward the brain (Fig.8B,D,F,H). Quantifications in Ascl-1 KOs revealed a significant (~86%) decrease in the total number of GnRH-1 immunoreactive cells (Fig.8Q). Immunostaining against Sox10 revealed that the reduced number of olfactory and vomeronasal axonal bundles in the nasal area were surrounded by OECs. Mucosal OECs were localized proximal to the basal lamina of the OE and VNO (Fig.8K-N,P).

These data indicate that Ascl-1 loss-of-function compromises GnRH-1 development but still can support GnRH-1ns differentiation and cell migration. As we observed a severe reduction in the number of GnRH-1ns in Ascl-1 null mutants, but not in Gli3$^{Xt/Xt}$, our data suggest that the mechanisms controlling Ascl-1 expression in GnRH-1 neuronal progenitors is Gli3 independent. Moreover, we found no olfactory tangles in the nasal area of Ascl-1 KOs. These Sox10 positive OECs reside along the olfactory bundles spanning from the olfactory mucosa (62). These observations suggest that loss of OECs in Gli3$^{Xt/Xt}$ mutants is not just an indirect effect of the reduced olfactory/vomeronasal neurogenesis, but rather indicates either a neural crest defect or a lack of expressed inductive signals in the olfactory and vomeronasal cells required to induce OECs maturation (50, 62).

### An unidentified *GLI3* loss-of-function mutation in a patient presenting with KS and polydactyly.

Since KS is associated with reproductive failure and features a hallmark of defects in GnRH-1 neuronal migration, we examined the genetic constraint for GLI3 gene in Genome Aggregation Database (gnomAD) (90). This population genetics data showed that GLI3 human genetic variants were highly constrained for loss-of-function variants with an observed/expected score metric of 0.09, suggestive of a strong intolerance to loss-of-function variants reflecting the strength of selection acting on heterozygotes. So, we queried WES data from 632 KS probands for *GLI3* loss-of-function variants. We identified two qualifying GLI3 loss-of-function variants from WES data, which identified a previously unidentified heterozygous *GLI3* loss-of-function (frameshifting indel) variant (c.1161del; p.P388Qfs*13; minor allele frequency in gnomAD: 0). This was confirmed by Sanger sequencing in a KS male subject. Additional KS/nIHH gene analysis showed that this KS proband also harbored a heterozygous *GNRHR* missense mutation (p.Q106R). Since gnomAD variants are not Sanger-confirmed, we performed a gene-based burden test between the KS cohort and gnomAD for all qualifying *GLI3* loss-of-function variants that showed enrichment in the KS cohort (p=0.002). We did not observe this enrichment when correcting for Sanger-confirmed variants only in the KS cohort but retaining all unconfirmed gnomAD variants (p=0.06).

The patient harboring the *GLI3* loss-of-function variant is a 38-year-old male, who presented to medical attention at age 18 years with anosmia and failure to enter puberty. He was undervirilized with a bilateral low testicular volume (8 ml). His biochemical investigations showed frank hypogonadotropic hypogonadism (serum testosterone: 67 ng/dL; LH: 2.1 mIU/mL and FSH: 3.9 mIU/mL), and his UPSIT showed complete anosmia, confirming a clinical diagnosis of Kallmann Syndrome. Notably, in keeping with the well-established role of GLI3 in limb development, he reported in his history an extra toe on his right foot, for which he underwent surgery as a child, and bilateral webbed toes (2nd and 3rd toes). To test the biological effects of the identified GLI3 variant, we performed a luciferase assay (Fig.9) to compare the activity of Wild type (WT) GLI3 and mutated GLI3 using a reporter plasmids containing wildtype GLI binding site linked to firefly luciferase (WTGliBS-Luc). A reporter carrying a mutated/nonfunctional (MutGLiBS-Luc) Gli3 binding site linked to firefly luciferase (63, 64) was used as negative control. Notably luciferase assay on HeLa cells (ATCC CCL-2) revealed, in contrast with what previously published by others (65), that Gli3 acts a transcriptional repressor. This analysis demonstrated the deleterious loss-of-function nature of our novel *GLI3* frameshift mutation (p.P388Qfs*13), which affected the repressor ability of Gli3, consistent with a GLI3 loss-of-function as a putative mechanism for GLI3-related KS.

## Discussion

In this study, we examined Gli3 loss-of-function on the development of olfactory placodal derivatives, such as the vomeronasal sensory neurons, terminal nerve and GnRH-1 neurons. We found that Gli3 loss-of-function leads to: 1) loss of Ascl-1 neuronal progenitors in the VNO and a dramatic reduction in the number of vomeronasal sensory neurons (VSNs), 2) a near complete absence of GnRH-1 neuronal migration to the brain, 3) aberrant formation of OECs in the nasal mucosa associated with defective development of terminal nerve fibers (TN) and 4) loss of forebrain expression of

Semaphorin 3A (Sema3A), a key axonal guidance molecule that controls GnRH-1 migration in the brain (45, 47, 66). Using WES data from a large cohort of KS patients, we identified a novel GLI3 loss-of-function mutation in a KS patient, who also displayed polydactyly. Luciferase assays of the mutant GLI3 protein confirmed loss of repressor function, which confirmed the pathogenicity of the identified *GLI3* loss-of-function mutation. Based on our results, we conclude that the lack of functional Gli3 transcriptional control compromises vomeronasal neurogenesis, terminal nerve development and OECs formation in the nasal area, which prevents GnRH-1 neuronal migration to the brain. By examining Gli3$^{Xt/Xt}$ mouse mutants, we also found dramatic changes in Sema3A expression in the brain. Notably, we only observed a delay in GnRH-1 migration in Gli3$^{Xt/WT}$ heterozygous embryos with no GnRH-1 defects observed after birth.

Shh signaling plays important roles in many developmental events, including cell specification, migration, innervation, and neurogenesis. In the absence of Shh signaling, the default function of Gli3 is repressing Shh target genes. Analyzing Gli3 expression in the developing olfactory pit, we observed that, as in the brain cortex (17), Gli3 is mostly expressed in proliferative Hes-1 positive cells. Hes-1 represses Ascl-1 expression in undifferentiated/proliferative neuroepithelial cells (39, 67, 68). Analysis of developing vomeronasal sensory neurons in Gli3$^{Xt}$ null mutants showed a dramatic reduction for both apical and basal VSNs secondary to a nearly complete loss (~91%) of Ascl-1 positive neurogenic progenitors in the VNO. Surprisingly, the number of GnRH-1ns did not appear different form WT controls. These results indicate that loss of Gli3 mediated gene repression negatively regulates the onset of vomeronasal neurogenic progenitors but not GnRH-1 neurogenesis.

Understanding the mechanisms that underlies how Gli3 loss compromises neurogenesis in the developing olfactory pit requires further investigation. However, the cell cycle duration of ectodermal derived neuroepithelial cells can control the shift from proliferative to neurogenic cell divisions (69, 70). Cyclin-dependent kinase gene *Cdk6* was recently identified as a direct target of Gli3 mediated repression (17). Loss of Gli3 expression in cortical neuroepithelial cells elevated Cdk6, which shortened the cell cycle and reduced neurogenesis (17, 70). Even though we detected Gli3 in Hes-1 proliferative cells, we propose that GLi3 utilizes a similar mechanism to that described in the cortex (17). Gli1 is only expressed in response to Shh, when Gli3 transitions from being a transcriptional repressor to a transcriptional activator. We performed Gli1 immunostaining on the developing VNO and did not find Gli1 expression (data not shown). This finding suggests that Gli3 acts as a transcriptional repressor in proliferative cells of the developing VNO. Notably, Gli3 heterozygous mutant mice showed a small delay in GnRH-1 migration during development, but they showed no differences in cell number or distribution after birth and were fertile. These data suggest that only heterozygous Gli3 loss-of-function mutations cannot produce a GnRH-deficient state in mice, which is consistent with results from Gli3 hypomorphic mutant mice (51)

## Gli3$^{Xt/Xt}$ mutants lack olfactory ensheathing cells in the nasal mucosa.

By analyzing the migration of GnRH-1ns in Gli3 mutants, we found that most GnRH-1 cells were unable to migrate far from the vomeronasal organ and formed large clumps of cells on tangled Nrp1+ fibers of the putative Terminal nerve. These data suggest that Gli3 loss-of-function compromises the ability of the TN to extend its neurites towards the brain and/or the ability of GnRH-1ns to migrate, a phenotype resembling that of Sox10 null mutants (3, 4). OECs are a glial population that wraps bundles of olfactory and vomeronasal axons from their epithelia to their central synaptic targets (50). OECs like Schwann cells arise from Sox10 positive precursors deriving from the neural crest (49, 50, 62, 71, 72). OECs are crucial players in controlling terminal nerve trajectory and GnRH-1 neuron migration from the nasal area to the brain (3, 4, 73). Gli3 can act as a Sox10 modifier, which suggests that Gli3 loss-of-function can compromise the development of neural crest derivatives such as melanocytes (34). Here we observed that Gli3 loss impairs normal formation of OECs in the nasal mucosa, as we found virtually no Sox10 positive cells in the olfactory/vomeronasal bundles of Gli3$^{Xt}$ null mutants nor proximal to the basal lamina and lamina propria of the olfactory epithelia (74). In Gli3$^{Xt/Xt,}$ Sox10+ Schwann cells were found around the trigeminal nerve (Fig.5) and Grueneberg ganglion (data not shown). We also found Sox10 positive OECs surrounding the FCM proximal to the olfactory bulbs. These intriguing data suggest the existence of developmental differences between OECs of the nasal mucosa and olfactory bulb OECs (74-76).

### Gli3$^{Xt/Xt}$ dysmorphic forebrain lacks Sema3A expression.

In addition to the tangling of TN fibers and impaired migration of GnRH-1ns in the nasal area, we observed that Gli3 mutants showed sporadic TN and GnRH-1 cells could migrate to the brain but not invade it. These findings revealed a similar cellular behavior to that described after Sema3A loss-of-function. Detailed analyses of Gi3$^{Xt/Xt}$ mutants confirmed very dysmorphic forebrain structures with expanded regions positive for the early subpallial marker, GAD1, and ectopic olfactory bulbs (25, 29, 52, 54). Notably in-situ hybridization against Sema3A showed a nearly complete absence of Sema3A expression in the forebrain, a condition that alone is not permissive for normal GnRH-1 migration (45). This finding indicates uncovering if the altered Sema3A expression observed in Gli3 mutants directly depends on the lack of functional Gli3 transcriptional control or reflects overall aberrant brain development.

### Ascl-1$^{null}$ mutants only partially recapitulate the Gli3$^{Xt/Xt}$ phenotype.

Ascl-1 null mutants revealed a previously unidentified role for Ascl-1 in controlling GnRH-1 neurogenesis, as we found an approximate 86% in the number of GnRH-1 neurons. These data challenge a previous proposal (62). Our data instead indicate a role for bHLH factors in controlling the genesis of GnRH-1ns (61). However, the lack of overlapping phenotype between Gli3$^{Xt}$ null (normal GnRH-1 but reduced VSN cell numbers) and Ascl-1 null mutants (both reduced GnRH-1 and VSNs cell numbers) indicates that Ascl-1 is not regulated in a Gli3 dependent fashion. We also found the few GnRH-1ns could migrate along sparse peripherin positive axonal bundles in Ascl-1 mutants. By analyzing OECs development in Ascl-1 null mutants, we detected OECs in the nasal mucosa associated with sparse peripherin positive bundles. Based on these data, we conclude that the lack of OECs in the nasal mucosa of Gli3$^{Xt/Xt}$ mutants does not solely reflect the reduced inductive signals arising from the decreased number of olfactory and vomeronasal fibers (62).

### *GLI3* mutations contribute to KS pathogenesis in humans

We identified a novel *GLI3* frameshifting loss-of-function variant in a KS proband. Using site-directed mutagenesis and luciferase assays, we confirmed a loss of repressor ability of this mutation to decrease the repressor ability of GLI3, which confirmed functional deleteriousness effects. Notably, this patient also displayed polydactyly and syndactyly, two hallmark clinical features of humans with *GLI3*-Greigs cephalopolysyndactyly syndrome (GCPS), which corresponds to the loss of Gli3 transcriptional repression during limb development (26, 77). Further, the identified *GLI3* loss-of-function variant (p.P388Qfs*13) affects the 5' part of the *GLI3* gene that leads to a truncation upstream of the zinc finger domain and is well-correlated with GCPS phenotype (26, 77). Reviewing previously reported *GLI3* mutation subjects with GCPS or oral-facial-digital syndrome indicates that a small minority of these patients also display micropenis (26, 78), cryptorchidism (26, 78), or anosmia (26). These phenotypes are consistent with underlying KS. KS/HH may be under-recognized in these reports, as reproductive phenotypes cannot be assessed in pre-pubertal subjects harboring *GLI3* mutations. Taken together, these observations implicate heterozygous *GLI3* loss-of-function mutations as a contributing genetic factor for KS/HH, which is further supported by the association of *GLI3* missense variants in two subjects with nIHH (32). Further, Gli3$^{Xt/Xt}$ mutant mice also display defective development of OECs and altered Sema3A, which are implicated in the pathogenesis of human KS (3, 47).

However, we did not observe any overt reproductive phenotypes in heterozygous Gli3$^{XtXt}$ mice. This discordance between human and mouse phenotypic characteristics is noted for other KS/HH genes, suggesting that the genetic architecture of human KS seems distinct compared to murine GnRH ontogeny. We acknowledge that heterozygous *GLI3* mutations *per se* may be insufficient to cause KS/HH and may require additional genetic or non-genetic modifiers. Indeed, KS has a well-established oligogenic basis (79). Here we found the GLI3 loss-of-function mutation was associated with an additional rare *GNRHR* p.Q106R missense mutation. Although the *GNRHR* p.Q106R variant can be deleterious in cellular assays (80), *GNRHR* mutations typically cause autosomal recessive hypogonadotropic hypogonadism (81). So, the occurrence of *GLI3* and *GNRHR* variants in this proband suggests a potential oligogenic (*GLI3/GNRHR*) contribution to the pathogenesis of the underlying KS. These compelling findings highlight an area for future study with other independent KS cohorts.

In summary, we revealed a crucial role for Gli3 in controlling the neurogenesis of vomeronasal sensory neurons, the formation of OECs in the nasal mucosa and the migration of GnRH-1 neurons. Our findings indicate an active role for Gli3 in triggering the transition from a proliferative to neurogenic program in the developing VNO. Since we found a dramatic reduction in the number of Sox10 expressing OECs and aberrant Sema3A in the brain, we propose that Gli3 acts as a genetic modifier and contributes to the oligogenic nature of KS/iIHH. Future studies will further investigate the gene regulatory network controlled by the Gli3 transcriptional network in the developing nasal olfactory system and identify KS/HH candidate genes to confirm the role of this transcription factor as a modifier in the oligogenic nature of KS/niHH.

## Material and Methods

**Animals**: Gli3$^{Xt}$ (82) and Ascl-1$^{tm1.1(Cre/ERT2)Jeo}$/J mice (83) on C57BL/6J background were purchased from (Jackson Laboratories, Bar Harbor, ME). Both colonies were maintained on C57BL/6J. The genotypes of Gli3$^{Xt}$ mice were established by PCR analysis using the following primers: Gli3-C3F: GGCCCA AACATCTACCAACACATAG, Gli3-C3R: GTTGGCTGCTGCATGAAGACTGAC; Gli3-XtJ580F: TACCCCAGCAGGAGACTCAGATTAG; Gli3-XtJ580F: AAACCCGTGGCTCAGGACAAG. Ascl-1$^{CreERT2}$ were genotyped following Ascl-1$^{tm1.1(Cre/ERT2)Jeo}$/J protocol available on jax.org website. Amplification products were analyzed by agarose gel electrophoresis. Animals were euthanized using CO2, followed by cervical dislocation. Mutant and wild-type mice of either sex were used. All mouse studies were approved by the University at Albany Institutional Animal Care and Use Committee (IACUC).

**Tissue preparation**: Embryos were collected from time-mated dams where the emergence of the copulation plug was taken as E0.5. Collected embryos were immersion-fixed in 3.7% Formaldehyde/PBS at 4°C for 3-5 hours. Postnatal animals were perfused with 3.7% Formaldehyde/PBS. All samples were then cryoprotected in 30% sucrose overnight, then frozen in O.C.T (Tissue-TeK), and stored at -80ºC. Samples were cryosectioned using CM3050S Leica cryostat and collected on Superfrost plus slides (VWR) at 12-16μm thickness for immunostainings and 18-25μm for *in situ hybridizations (ISH)*.

**Immunohistochemistry:** Primary antibodies and dilutions used in this study were: goat-α-neuropilin-2 (1:3000, R&D Systems), goat-α-neuorpilin-1 (1:400, R&D Systems), mouse-α-ROBO2(1:50, Santa Cruz) chicken-α-peripherin (1:1500, Abcam), rabbit-α-peripherin (1:2000, Millipore), SW rabbit-α-GnRH-1 (1:6000, Susan Wray, NIH), goat-α olfactory marker protein (1:4000, WAKO), mouse -α-GAD67 (1:200, Santa Cruz), goat-α-AP-2ε (1:1000, Santa Cruz), mouse-α-Meis2 (1:500, Santa Cruz), rabbit-α-phospho-Histone-H3 (1:400, Cell Signaling), rat-α-phospho-Histone-H3 (1:500, Abcam), goat-α-Sox10 (1:100, Santa Cruz), goat-α-collagen IV (1:800, Millipore), goat-α-Gli3 (1:200, R&D

Systems), rabbit-α-Hes-1 (1:200, Cell Signaling), and mouse-α-Ascl-1 (1:30, Santa Cruz). Antigen retrieval was performed in a citrate buffer prior to incubation with chicken-α-peripherin, rabbit-α-phospho-Histone-H3, rat-α-phospho-Histone-H3, goat-α-AP-2ε, mouse-α-Meis2, goat-α-Gli3, rabbit-α-Hes-1, mouse-α-Ascl-1, goat-α-Sox10, mouse-α-ROBO2, and mouse-α-GAD67 antibodies. For immunoperoxidase staining procedures, slides were processed using standard protocols (37) and staining was visualized (Vectastain ABC Kit, Vector) using diaminobenzidine (DAB) in a glucose solution containing glucose oxidase to generate hydrogen peroxide; sections were counterstained with methyl green. For immunofluorescence, species-appropriate secondary antibodies were conjugated with Alexa-488, Alexa-594, or Alexa-568 (Molecular Probes and Jackson Laboratories) as specified in the legends. Sections were counterstained with 4′,6′-diamidino-2-phenylindole (1:3000; Sigma-Aldrich) and coverslips were mounted with Fluoro Gel (Electron Microscopy Services). Confocal microscopy pictures were taken on a Zeiss LSM 710 microscope. Epifluorescence pictures were taken on a Leica DM4000 B LED fluorescence microscope equipped with a Leica DFC310 FX camera. Images were further analyzed using FIJ/ImageJ software. Each staining was replicated on at least three different animals for each genotype

**In situ hybridization**: Digoxigenin-labeled cRNA probes were prepared by in vitro transcription (DIG RNA labeling kit; Roche Diagnostics) from the following templates: Semaphorins 3A (84), Gli3 riboprobe RP_080717_03_E04 (Forward primer GCAGAATTATTCCGGTCAGTTC ; Reverse primer TCAGTCTTTGTGTTTGTGGTCC). In situ hybridization was performed as described (42) and visualized by immunostaining with an alkaline phosphatase conjugated anti-DIG (1:1000), and NBT/BCIP developer solution (Roche Diagnostics). Sections were then counter-immunostained with antibodies against both chicken-α-peripherin, and SW rabbit-α-GnRH-1, as described above for immunofluorescence.

**Cell quantifications**: Quantification of GnRH-1 neuronal distribution in mutant and control animals was performed in the nasal region (VNO, axonal tracks surrounding the olfactory pits), forebrain junction and brain (all the cells that accessed the olfactory bulb

and were distributed within the forebrain). Number of cells were calculated for each animal as the average of the counted cells per series multiplied by the number of series cut per animal. Differences at each interval between genotypes was assessed by unpaired t-Test.
Number of vomeronasal apical and basal neurons was counted after AP-2ε and Meis2 immunostaining, as cells/section on an average of 4 sections/embryo. Progenitors cells were counted after immunostaining for Phospho-Histone H3, Ascl-1, and Hes-1 and were quantified as described above for vomeronasal cells. Sox10 positive cells were quantified in a 334,500 $\mu m^2$ field area for an average of 4 VNO sections per animal, only Sox10 positive cells proximal to the VNO were counted. Means ± SEs were calculated on at least three animals per genotype, *t* test was used to assess differences between groups.

**Densitometric Analysis of the Median Eminence**: Brains of 5-month-old male $Gli3^{Xt}$ WT and heterozygous mice (n=3;3) were cryosectioned coronally at 20μm. Three series for each animal were stained for GnRH in DAB. Brightfield images of comparable sections for each series were taken for quantification. Images were processed with color deconvolution and the mean gray value was measured for a standardized ROI to calculate the average optical density for each animal.

**Site directed mutagenesis**: The GLI-3 bs-2 plasmid carrying the human GLI3 (85) was purchased from Addgene. F387F*fs mutation was generated in the vector pCDNA3 hGli3 using Q5 site directed mutagenesis kit (NEB) using primers Gli3 F387Ffs* Fwd CCAACACAGAGGCCTATTCC and Gli3 F387Ffs* Rev AAAGTTGGGGCAGGGTGG following the manufacturer’s instruction. Mutation was validated by sequencing prior to use in experiments.

**Transfection and luciferase reporter assay**: $1x10^4$ HeLa cells (ATCC) were seeded into a 96-well plate 24 hours before transfections. 100 ng of either reporter plasmid (8 X 3 GLI-BS Luc or 8 X 3 Mut GLI-BS Luc) and 100 ng of the effector plasmid (hGli3 WT or F387F*fs) and 20 ng of pRL-SV40 were co-transfected using Lipofectamine 3000

(ThermoFisher). pRL-SV40 coding for *Renilla* luciferase was used as a transfection control and for normalization. Cells were harvested 48 hours post transfection and Firefly and *Renilla* luciferase intensities were measured using Glomax 96 microplate luminometer (Promega) and dual-Luciferase Reporter Assay System (Promega).

**WES analysis of KS individuals for GLI3 loss-of-function mutations**: A total of 632 KS subjects at the Harvard Reproductive Endocrine Sciences Center were examined for *GLI3* loss-of-function mutations in this study. KS was defined by: (i) absent or incomplete puberty by age 18y; (ii) serum testosterone <100 ng/dL in men or estradiol<20 pg/mL in women in the face of low or normal levels of serum gonadotropins; (iii) otherwise normal anterior pituitary function; (iv) normal serum ferritin concentrations; and (v) normal MRI of the hypothalamic-pituitary region (86); and (v) impaired olfaction as determined by the University of Pennsylvania Smell Identification Test (UPSIT) (87, 88). Clinical charts and patient questionnaires of KS subjects were reviewed for phenotypic evaluation. Whole exome sequencing (WES) data in the KS cohort was performed on peripheral blood-derived DNA using either Nimblegen SeqCap target enrichment kit (Roche) or a custom Illumina capture kit (ICE) and the detailed variant-calling and annotation used have been described previously (89). WES data were then queried for *GLI3* (RefSeq: NM_000168.6) loss-of-function variants: defined as those variants resulting in protein alteration in the canonical *GLI3* transcript as determined by Variant Effect Predictor (VEP) (127), resulting in nonsense, and essential splice site mutations; or (b) indels resulting in frame-shift mutations; AND (b) with ethnicity-specific minor allele frequency (MAF) <0.1% minor allele frequency (MAF) in gnomAD database (http://gnomad.broadinstitute.org) (90) . To ascertain oligogenicity, KS proband(s) with *GLI3* loss-of-function variants were also examined for rare sequence variants (RSVs) in other known KS/nIHH genes [*ANOS1* (NM_000216.4), *CHD7* (NM_017780.4), *FEZF1* (NM_001160264.2), *FGF8* (NM_006119.4), *FGFR1* (NM_023110.2), *GNRH1* (NM_000825.3), *GNRHR* (NM_000406.2), *HS6ST1* (NM_004807.3), *KISS1* (NM_002256.4), *KISS1R* (NM_032551.5), *NR0B1* (NM_000475.4), *NSMF* (NM_001130969.1), *PROK2* (NM_001126128.2), *PROKR2* (NM_144773.3), *SEMA3A* (NM_006080.3), *SMCHD1* (NM_015295.2), *SOX2* (NM_003106.4), *TAC3* (NM_013251.4), *TACR3* (NM_001059.3), and *WDR11* (NM_018117.12)]. RSVs in these other HH genes were defined as single nucleotide variants resulting in protein alteration in canonical transcript as determined by Variant Effect Predictor (VEP) (127) resulting in missense, nonsense, and essential splice site mutations; or (b) indels resulting in frame-shift mutations; AND (b) with ethnicity-specific minor allele frequency (MAF) <1% in GnoMAD. Variants identified from above analysis were then confirmed by Sanger sequencing.

**Statistical Analyses**. All statistical analyses were carried out using GraphPad Prism7 software. Cell counts were done on serial sections immunostained for GnRH-1 at E13.5 (n=3) and E15.0 (n=4) and visualized under bright field (immunoperoxidase) or epi-fluorescence illumination (20×; Leica DM4000 B LED), according to their anatomical location [*i.e.,* (1) nasal region (VNO, axonal tracks surrounding the olfactory pits, forebrain junction); (2) olfactory bulb/fibrocellular mass; and (3) brain (all the cells that accessed the olfactory bulb and were distributed within the forebrain)]. For each animal, counts were performed on 3 serial series. The average number of cells from these 3 series was then multiplied by the total number of series/animal to compute a value for each animal. These were then averaged ± standard error (SE) among animals of the same age and genotype. Means ± SEs were calculated on at least three animals per genotype. The statistical difference between genotypes and groups were determined using an unpaired student's t-test. A gene-based burden testing for human *GLI3* variants was performed between the KS and the gnomAD using a Fisher's-exact test. All data are represented as the mean ±SEM from n≥3 mice per genotype/age for each experiment. Values of $p < 0.05$ were considered to be statistically significant.

## Author contributions

ET, AN, JL, NP, EG, GF, conducted the experiments and performed data analysis, PF and GF performed data analysis designed the experiments, ET, RB and PF wrote the paper, GF, RB and DK shared reagents, performed data analysis and edited the paper.

## Acknowledgments

We thank Dr. Hirotomo Saitsu (Hamamatsu University School of Medicine, Hamamatsu, Japan) for sharing Gli3 luciferase reporter plasmids and Dr. Susan Wray for sharing the anti GnRH-1 (SW) antibody.

Research reported in this publication was supported by the Eunice Kennedy Shriver National Institute of Child Health and Human Development of the National Institutes of Health under the Award Numbers 1R15HD09641101 (PF), and 1R01HD097331-01 (PF) and by the National Institute of Deafness and other Communication Disorders of the National Institutes of Health under Award Number 1R01DC017149-01A1 (PF). RB is supported by the Eunice Kennedy Shriver National Institute of Child Health and Development (K23 HD077043; R01 HD096324; P50 HD HD028138). The content of this manuscript is solely the responsibility of the authors and does not necessarily represent the official views of the National Institutes of Health.

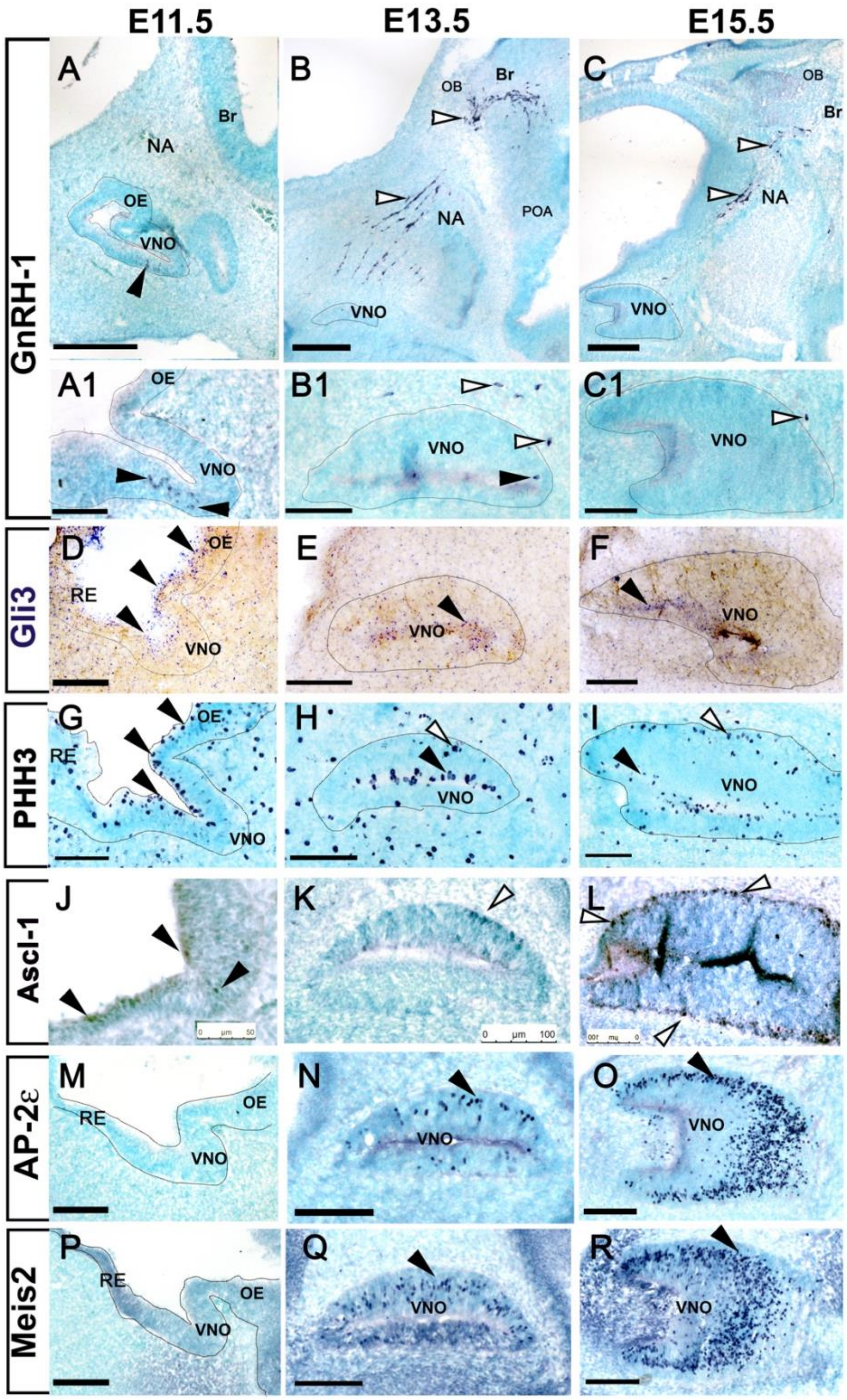
E11.5
E13.5
E15.5
GnRH-1
A
Br
NA
OE
VNO
B
OB
Br
NA
POA
VNO
C
OB
Br
NA
VNO
A1
OE
VNO
B1
VNO
C1
VNO
Gli3
D
OE
RE
VNO
E
VNO
F
VNO
PHH3
G
OE
RE
VNO
H
VNO
I
VNO
Ascl-1
J
0 µm 50
K
0 µm 100
L
M
AP-2ε
RE
OE
VNO
N
VNO
O
VNO
Meis2
P
RE
OE
VNO
Q
VNO
R
VNO

**Figure 1) Gli3 is expressed in the developing vomeronasal area.** GnRH-1ns can be detected at E11.5 (A,A1) in the ventral portion of the developing putative VNO and emerge from the VNO (white arrows) to the nasal area (NA) migrating toward the brain (Br) at E13,5 (B,B1) and E15.5 (C,C1). D-F Gli3 mRNA expression is detected in cells located in the apical portion of the developing olfactory pit and VNO (black arrows) at all analyzed stages. G-I) PHH3 immunoreactivity highlights dividing cells in the apical (black arrow) and basal (white arrows) regions of the developing VNO. J-L, immunostaining against Ascl-1 highlights sparse Ascl-1 positive cells at E11.5 (J), neurogenic Ascl-1+ cells were detected in the basal regions of the developing VNO at E13.5 and E15.5. Immunostaining against the basal transcription factor AP-2ε (M-O) and apical transcription factor Meis-2 (P-R) reveal the lack of detectable vomeronasal neurons at E11.5, while a growing number of neurons were detected between E13.5 and E15.5.

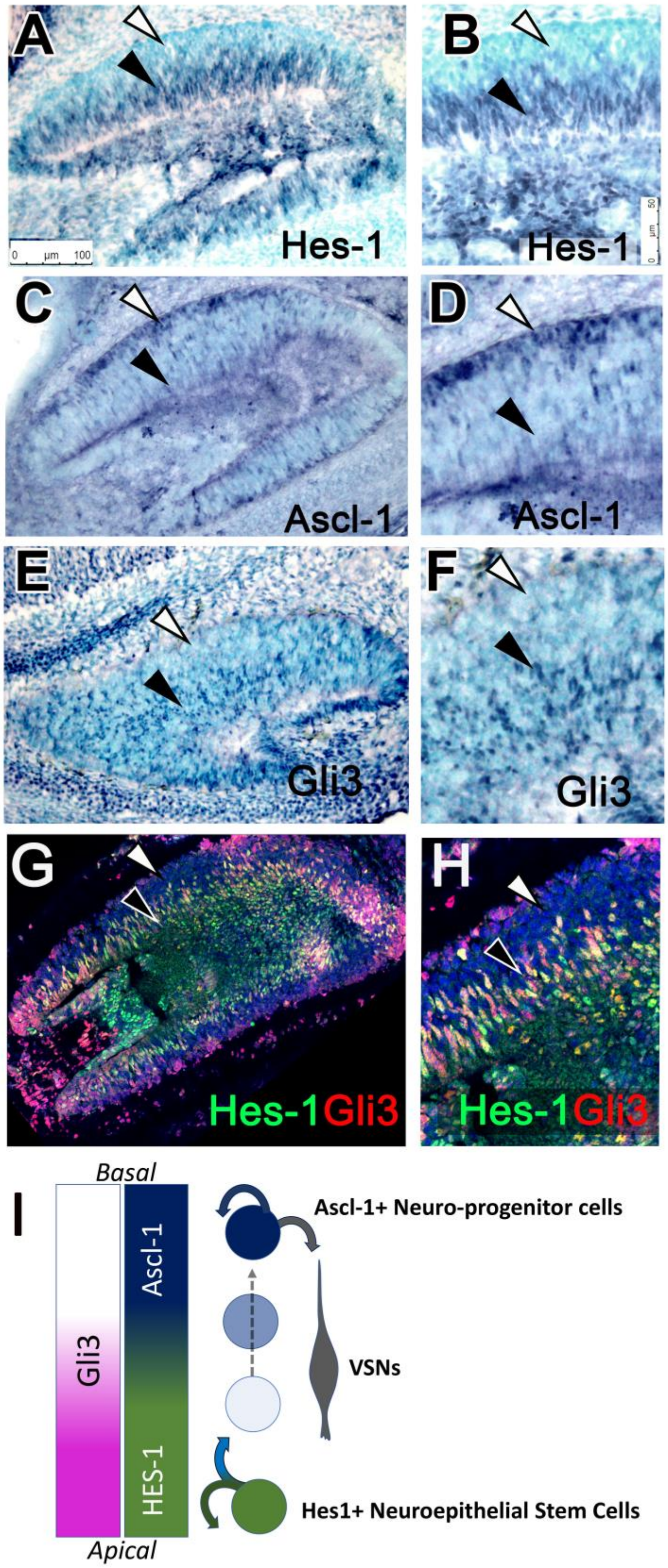
A
Hes-1
0 µm 100
B
Hes-1
0 µm 50
C
Ascl-1
D
Ascl-1
E
Gli3
F
Gli3
G
Hes-1Gli3
H
Hes-1Gli3
I
Basal
Gli3
Ascl-1
HES-1
Apical
Ascl-1+ Neuro-progenitor cells
VSNs
Hes1+ Neuroepithelial Stem Cells

**Fig.2 A) Gli3 is expressed in Hes-1, but not in Ascl-1, positive progenitors.**

E15.5 immunostaining against Hes-1 reveals Hes-1 expression in the cells located in the apical domains of the developing VNO (Black arrow). C,D) Immunostaining against Ascl-1 reveals expression of the neurogenic factor in cells in the basal territories of the developing VNO (White arrow), only background levels were found in the basal regions (Black arrow). E, F) Gli3 immunoreactivity was found in cells in the apical territories of the developing VNO (Black arrow). G-H) Double immunofluorescence against Gli3 and Hes-1 reveals strong Gli3 expression in the Hes-1 positive cells (Black arrow) and lack of immunodetectable Gli3 in the most basal levels (white arrow). I) Proposed model with Gli3 expression in proliferative Hes-1+ cells and in daughter cells that exit the proliferative program and enter the Ascl-1+ controlled pro-neurogenic program in the basal regions of the developing VNO.

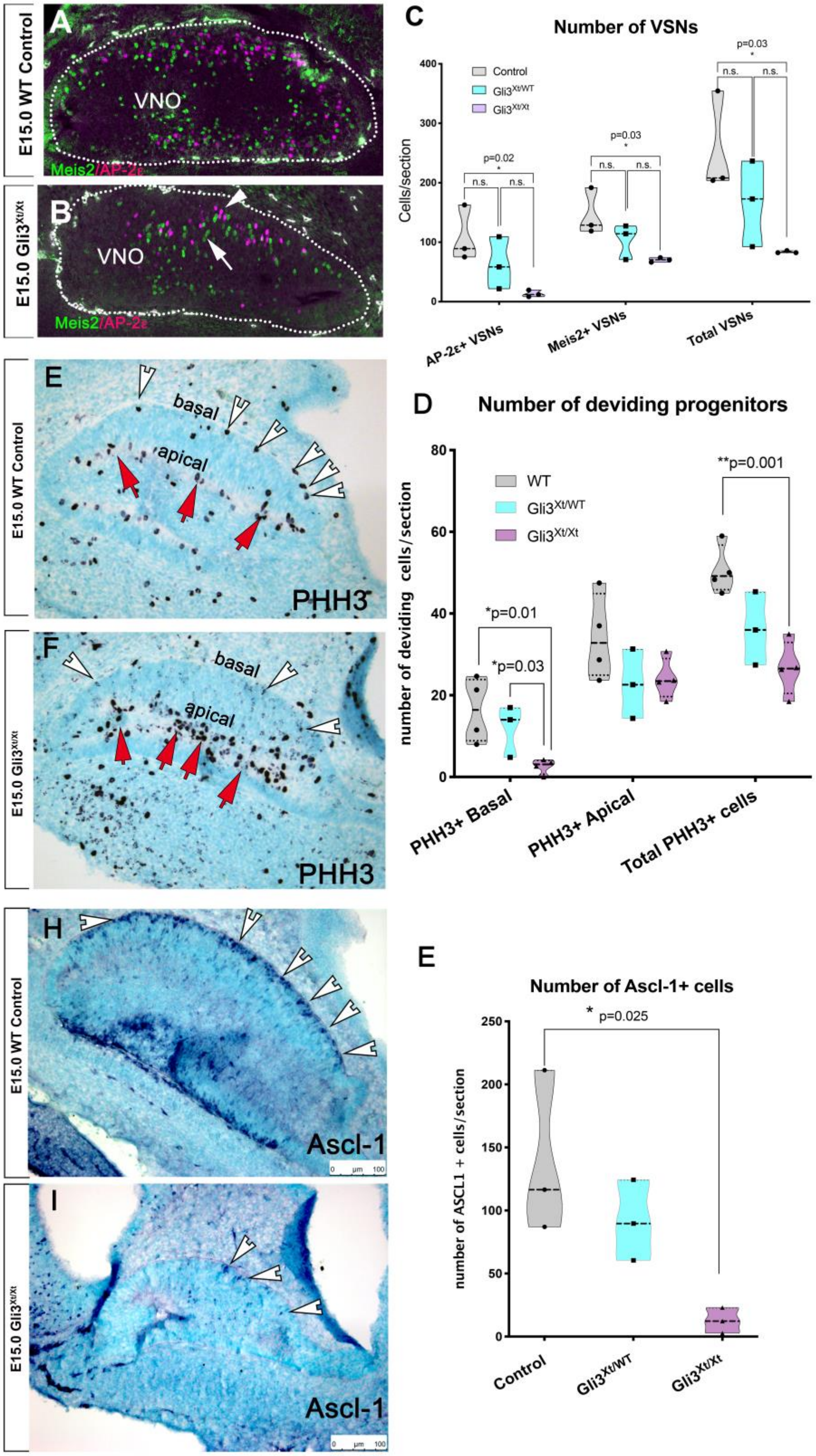
A
E15.0 WT Control
VNO
Meis2/AP-2ε
B
E15.0 Gli3Xt/Xt
VNO
Meis2/AP-2ε
C
Number of VSNs
Control
Gli3Xt/WT
Gli3Xt/Xt
Cells/section
0
100
200
300
400
p=0.02
*
n.s.
n.s.
p=0.03
*
n.s.
n.s.
p=0.03
*
n.s.
n.s.
AP-2ε+ VSNs
Meis2+ VSNs
Total VSNs
E
E15.0 WT Control
basal
apical
PHH3
F
E15.0 Gli3Xt/Xt
basal
apical
PHH3
D
Number of deviding progenitors
WT
Gli3Xt/WT
Gli3Xt/Xt
number of deviding cells/section
0
20
40
60
80
*p=0.01
*p=0.03
**p=0.001
PHH3+ Basal
PHH3+ Apical
Total PHH3+ cells
H
E15.0 WT Control
Ascl-1
0 µm 100
I
E15.0 Gli3Xt/Xt
Ascl-1
0 µm 100
E
Number of Ascl-1+ cells
* p=0.025
number of ASCL1 + cells/section
0
50
100
150
200
250
Control
Gli3Xt/WT
Gli3Xt/Xt

**Figure 3, Gli3 loss-of-function impairs the formation of Ascl-1+ neuronal progenitors, VSNs neurogenesis but not VSNs terminal differentiation** A,B) Immunostaining against the transcription factors Meis2 and AP-2ε highlights maturing apical and basal vomeronasal sensory neurons in controls (A) and Gli3$^{Xt/Xt}$ mutants (B). C) Quantifications of the average number of AP-2ε differentiated VSNs and Meis2 differentiated apical VSNs reveal a significant reduction in the number of differentiated VSNs in Gli3$^{Xt/Xt}$ mutants. E,F) PHH3 immunostaining and quantification (D) of VNO from WT and Gli3$^{Xt/Xt}$ reveals a reduction in the total number of dividing cells with a significant reduction of apical progenitors (white arrow), but not apical progenitors. H-I) Immunostaining against Ascl-1 in controls and Gli3$^{Xt/Xt}$ mutants reveals (E) a significant reduction in the number of Ascl-1 positive cells in the basal domains of the developing VNO.

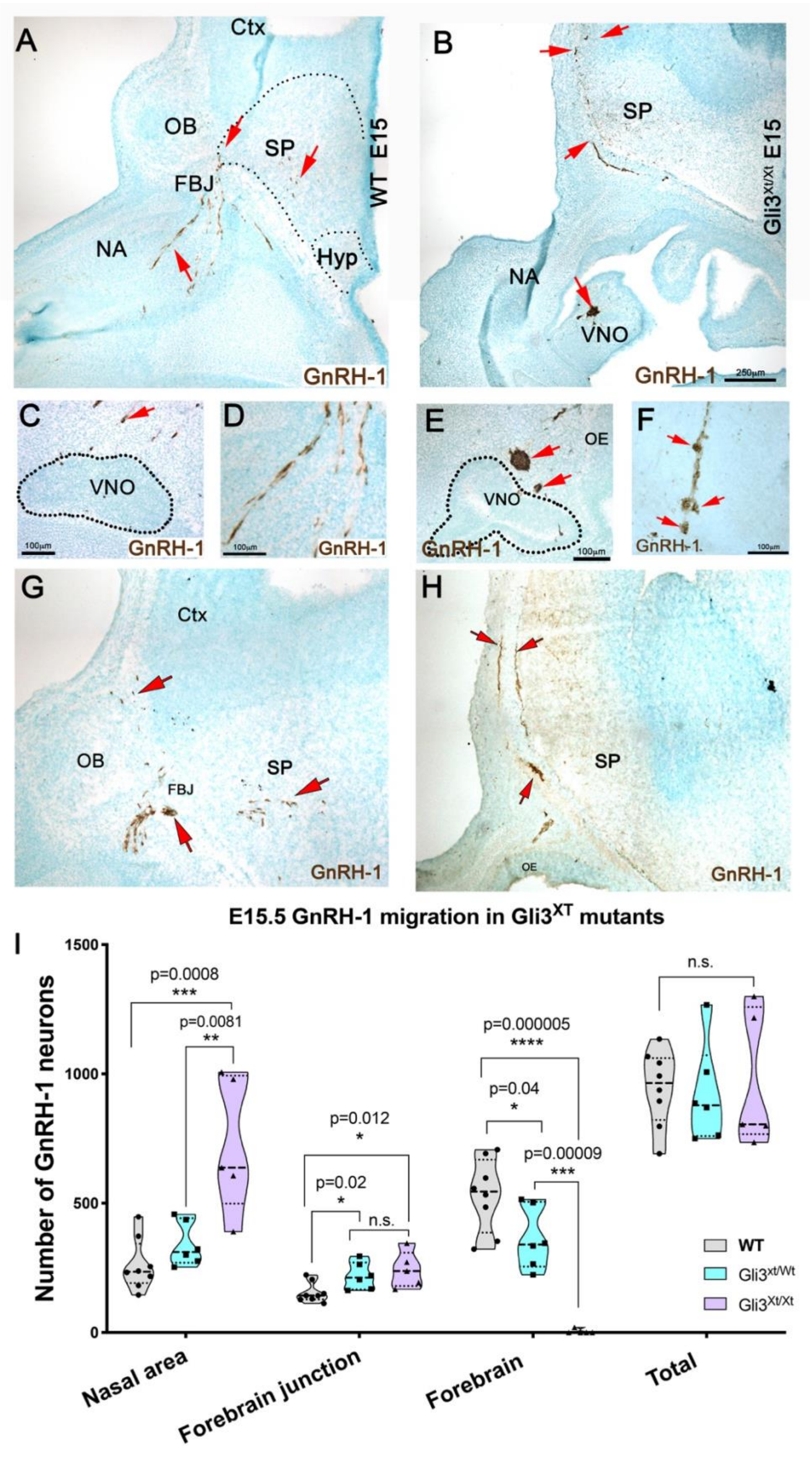
A
Ctx
OB
SP
FBJ
NA
Hyp
WT E15
GnRH-1
B
SP
Gli3Xt/Xt E15
NA
VNO
GnRH-1
250µm
C
VNO
100µm
GnRH-1
D
100µm
GnRH-1
E
OE
VNO
GnRH-1
100µm
F
GnRH-1
100µm
G
Ctx
OB
FBJ
SP
GnRH-1
H
SP
OE
GnRH-1
E15.5 GnRH-1 migration in Gli3XT mutants
I
Number of GnRH-1 neurons
1500
1000
500
0
p=0.0008
***
p=0.0081
**
p=0.012
*
p=0.02
*
n.s.
p=0.000005
****
p=0.04
*
p=0.00009
***
n.s.
WT
Gli3xt/Wt
Gli3Xt/Xt
Nasal area
Forebrain junction
Forebrain
Total

**Figure 4. Gli3$^{Xt/Xt}$ mutants display severely impaired GnRH-1 neuronal migration.** Representative images of immunostaining against GnRH-1 on WT (A-D) and Gli3$^{Xt/Xt}$ (E-H) at E15.5 (A) in WT controls. GnRH-1ns migrate as a continuum from the vomeronasal organ (VNO) to the brain. GnRH-1ns from the nasal area (NA), cross the forebrain junction (FBJ), invade the brain ventral to the OB, migrate through the subpallium (SP) to eventually reach the hypothalamic area (Hyp). B,C) GnRH-1ns migrating in the nasal area and out of the VNO. D) Detail showing GnRH-1ns invading the subpallium (SP) ventral to the OB in the region corresponding to the putative accumbens (Ac), some GnRH-1ns migrate to the cortex (Ctx) and around the olfactory bulbs (OBs). E-H) In Gli3$^{Xt/Xt}$, a large portion of GnRH-1ns neurons form clusters of cells proximal to the VNO while other migrate around the brain, occasional GnRH-1ns were found accessing the brain dorsal portion of the cortex (Ctx). F,G) GnRH-1 immunostaining (brown) show less organized GnRH-1ns forming clumps while migrating towards the brain (compare to B). G) Most of the GnRH- 1neurons form large clusters proximal to the VNO (arrows). H) Detail showing GnRH-1ns were unable to invade the brain migrating along the meninges. I) Quantification of the distribution of GnRH-1ns in WT, Gli3$^{Xt/WT}$ and Gli3$^{Xt/Xt}$. In Gli3$^{Xt/Xt}$ the majority of the GnRH-1ns remains in the nasal area. Both Gli3$^{Xt/WT}$ and Gli3$^{Xt/Xt}$ have a significant smaller number of GnRH-1ns in the brain compared to controls. Values ± SE, dots indicate numbers of embryos/genotype, unpaired t-test, significant values $p<0.05$.

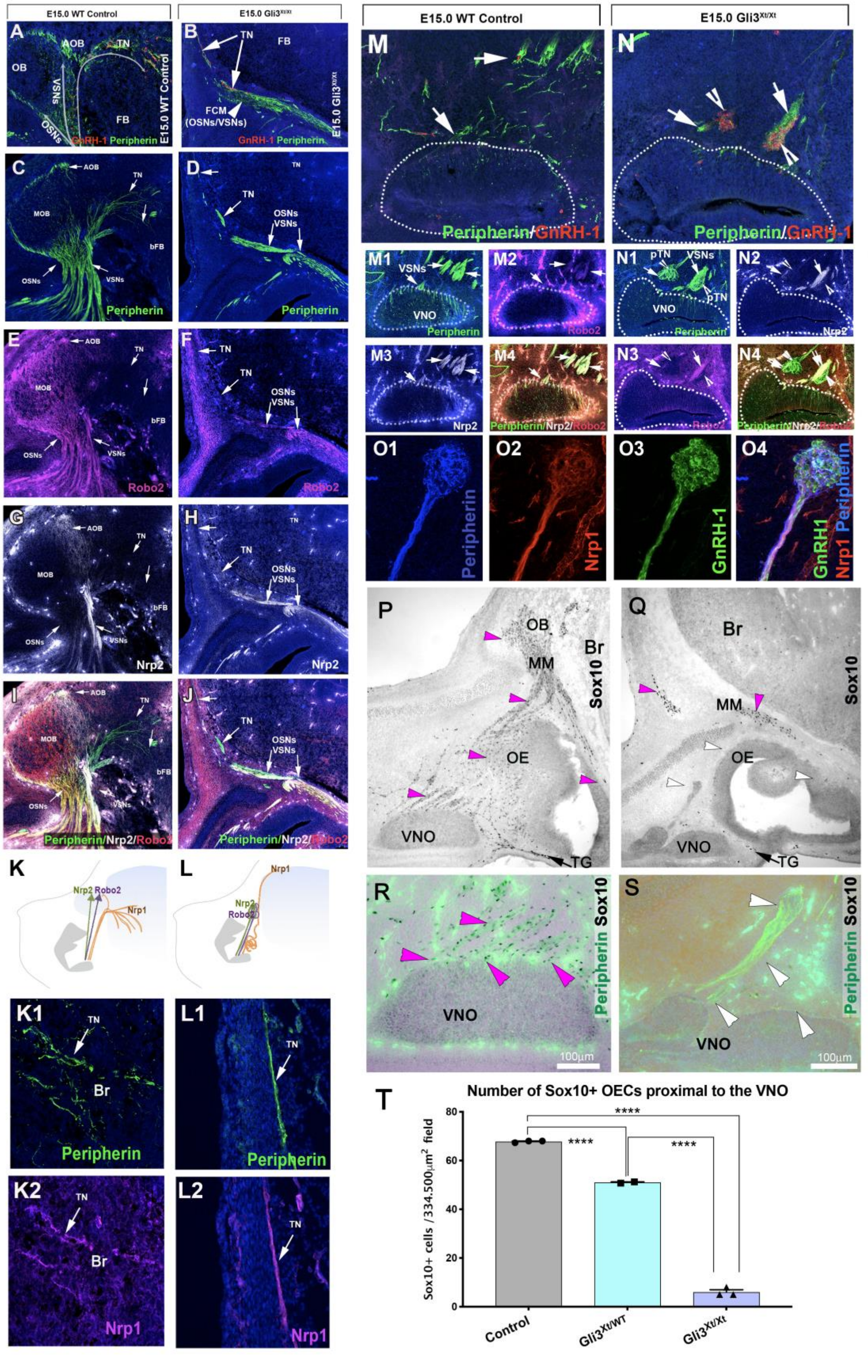E15.0 WT Control
E15.0 Gli3^Xt/Xt
E15.0 WT Control
E15.0 Gli3^Xt/Xt
A
AOB
TN
OB
VSNs
OSNs
FB
GnRH-1 Peripherin
E15.0 WT Control
B
TN
FB
FCM
(OSNs/VSNs)
GnRH-1 Peripherin
E15.0 Gli3^Xt/Xt
C
AOB
TN
MOB
bFB
OSNs
VSNs
Peripherin
D
TN
TN
OSNs
VSNs
Peripherin
E
AOB
TN
MOB
bFB
OSNs
VSNs
Robo2
F
TN
TN
OSNs
VSNs
Robo2
G
AOB
TN
MOB
bFB
OSNs
VSNs
Nrp2
H
TN
TN
OSNs
VSNs
Nrp2
I
AOB
TN
MOB
bFB
OSNs
VSNs
Peripherin/Nrp2/Robo2
J
TN
OSNs
VSNs
Peripherin/Nrp2/Robo2
K
Nrp2
Robo2
Nrp1
L
Nrp1
Nrp2
Robo2
K1
TN
Br
Peripherin
L1
TN
Peripherin
K2
TN
Br
Nrp1
L2
TN
Nrp1
M
Peripherin/GnRH-1
N
Peripherin/GnRH-1
M1
VSNs
VNO
Peripherin
M2
Robo2
N1
pTN
VSNs
VNO
pTN
Peripherin
N2
Nrp2
M3
Nrp2
M4
Peripherin/Nrp2/Robo2
N3
Robo2
N4
Peripherin/Nrp2/Robo2
O1
Peripherin
O2
Nrp1
O3
GnRH-1
O4
GnRH1 Nrp1 Peripherin
P
OB
MM
Br
Sox10
OE
VNO
TG
Q
Br
Sox10
MM
OE
VNO
TG
R
Peripherin Sox10
VNO
100µm
S
Peripherin Sox10
VNO
100µm
T
Number of Sox10+ OECs proximal to the VNO
Sox10+ cells /334.500µm² field
80
60
40
20
0
****
****
****
Control
Gli3^Xt/WT
Gli3^Xt/Xt

**Figure 5. Misrouted vomeronasal and terminal nerve axons in Gli3$^{Xt/Xt}$ are associated with lack ensheathing cells in the nasal mucosa.** A,C) Immunostainings against Peripherin and GnRH-1. B,D) Peripherin and GnRH-1 immunofluorescence, in Gli3$^{Xt/Xt}$ mutants the OSNs and VSNs form a fibrocellular cellular mass (FCM). The GnRH-1ns (D) and the TN do not remain in the FCM but migrate around the FB. C-I) WT E15.5, immunostaining against Peripherin, Robo2, Nrp2; the TN fibers are negative for Robo2expression and negative for Nrp2 see merge in I. D-J) Gli3$^{Xt/Xt}$ E15.5 immunostaining against Peripherin, Robo2, and Nrp2 and merge. K,L) Schematic of the phenotypes and fiber immunoreactivity in controls and Gli3$^{Xt/Xt}$ mutants. K1,K2) Immunofluorescence showing Neruopilin1 immunoreactivity in TN fibers invading the brain in WT embryos. L1,L2) Peripherin and Neruopilin1 positive fibers of the putative TN project around the brain. M-M4) In control animals the GnRH-1ns migrate along Peripherin positive bundles (M1), also immune reactive for Robo2 (M2), Nrp2 (M3), Merge in M4. In Gli3$^{Xt/Xt}$, GnRH-1ns form large clumps of cells suggesting disorganized Peripherin positive fibers. Some tangled fibers of the putative terminal nerve (N1) are negative for Nrp2 (N2) and Robo2 (N3). Merge in N4. O1-O4) In Gli3$^{Xt/Xt}$, tangles of putative TN fibers are positive for peripherin (O1) and Nrp1 (O2) and are associated with clusters of GnRH-1ns (O3). Merge in O4. P-S) GLI3$^{Xt/Xt}$ lack of OECs associated with the vomeronasal nerve. P-S) Combined Peripherin IF and Sox10 IHC. P) In controls, Sox10 immunoreactive OECs (magenta arrowheads) are found around the VNO, proximal to the basal lamina of the OE, along the Peripherin positive vomeronasal and olfactory bundles and as part of the migratory mass (MM) in front of the brain. Sox10+ Schwann cells were found associated along nasal trigeminal projections (TG). Q) In Gli3$^{Xt/Xt}$ mutants, Sox10 immunoreactive OECs were neither found proximal to the basal portions of the VNO, olfactory epithelium nor along the vomeronasal and olfactory projections (white arrowheads). Notably Sox10 positive cells were found in the migratory mass (MM). As in controls Sox10+ Schwann cells were found associated along nasal trigeminal projections (TG). R,S) Magnifications of the VNO. R) In control animals Sox10 positive OECs were found proximal to the basal lamina of the VNO, along the vomeronasal bundles. S) In Gli3$^{Xt/Xt}$ Sox10+ OECs were rarely found in proximity of the basal lamina of the VNO and

along the vomeronasal/terminal nerve bundles (white arrowheads). T) Quantification of Sox10+ OECs around the VNO, ****$p<0.0001$

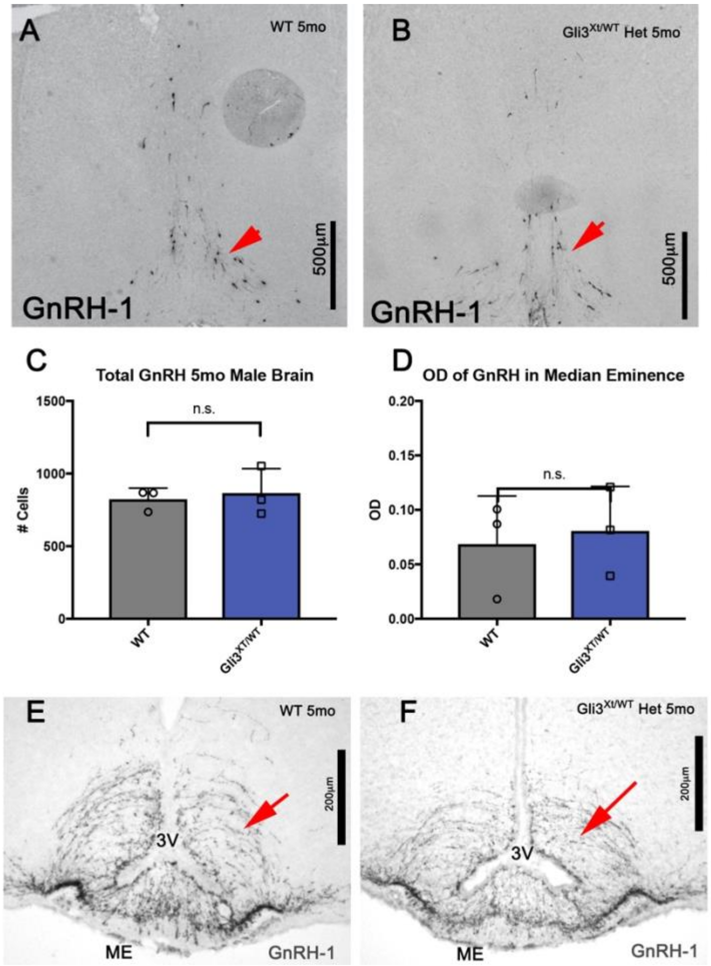
A
WT 5mo
500µm
GnRH-1
B
Gli3$^{Xt/WT}$ Het 5mo
500µm
GnRH-1
C
Total GnRH 5mo Male Brain
n.s.
# Cells
1500
1000
500
0
WT
Gli3$^{Xt/WT}$
D
OD of GnRH in Median Eminence
n.s.
OD
0.20
0.15
0.10
0.05
0.00
WT
Gli3$^{Xt/WT}$
E
WT 5mo
200µm
3V
ME
GnRH-1
F
Gli3$^{Xt/WT}$ Het 5mo
200µm
3V
ME
GnRH-1

**Figure 6. GLi3$^{Xt/WT}$ show no difference in GnRH-1ns numbers in the brain after birth.** A,B) Immunostaining against GnRH-1 on postnatal WT and Gli3$^{Xt/WT}$ heterozygous animals shows comparable immunoreactivity in GnRH-1 cell bodies in the preoptic area (arrows). C) Quantification for GnRH-1 immunoreactive cell bodies in the preoptic area indicates no statistical differences between controls and Gli3$^{Xt/WT}$ heterozygous mutants. D) Quantification of area occupied by GnRH-1 immunoreactive fibers in the median eminence of WT controls and Gli3$^{Xt/WT}$ heterozygous mutants. E,F). Representative images showing GnRH-1 immunoreactivity of GnRH-1 axons in the median eminence (ME) of WT and Gli3$^{Xt/WT}$ heterozygous mutants.

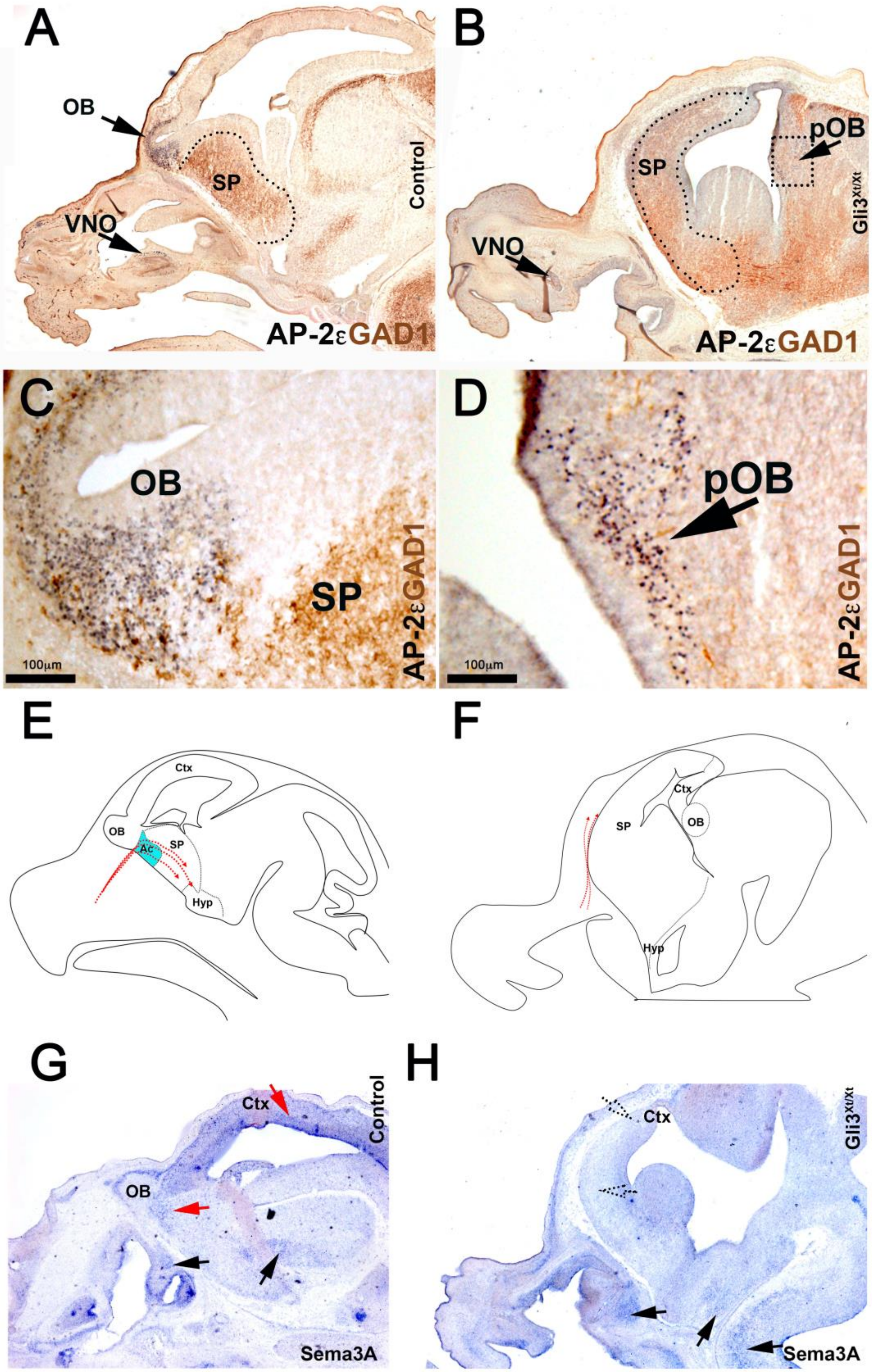
A
OB
SP
VNO
Control
AP-2ε GAD1
B
pOB
SP
VNO
Gli3$^{Xt/Xt}$
AP-2ε GAD1
C
OB
SP
100μm
AP-2ε GAD1
D
pOB
100μm
AP-2ε GAD1
E
Ctx
OB
Ac
SP
Hyp
F
Ctx
SP
OB
Hyp
G
Ctx
Control
OB
Sema3A
H
Ctx
Gli3$^{Xt/Xt}$
Sema3A

**Figure 7. Gli3$^{Xt/Xt}$ mutants display an expansion of expression of forebrain ventral markers, form ectopic olfactory bulbs and lack of Sema3A expression in the forebrain.** A) AP-2ε/GAD1 double immunostaining. Immunostaining against AP-2ε highlights mitral cells in the OB (magnified in C). GAD1 immunostaining highlights GABAergic neurons which are mostly located in the subpallium. B) In Gli3$^{Xt/Xt}$, AP-2ε highlight extopic mitral cells in the posterior portion of the forebrain (boxed, see magnification in (D) showing the ectopic AP-2ε+ OB in the poterior portion of the brain. GAD1 expression shows expansion of ventral forebrain maker. E-F) Illustration of GnRH-1ns migration in WT and Gli3 null animals. Area of Sema3A expression represented in light blue present in WT accumbens absent in the Gli3 KOs. G-H) In-situ hybridization against Sema3A shows detectable Sema3A expression in the nasal area, basal brain (black arrows) and hindbrain of control and Gli3 mutants. No Sema3A expression was detected in Gli3Xt mutants in the forebrain and cortex (compare red arrows in I with dotted arrows in H). Ac=accumbens, Ctx=cortex, Hyp=hypothalamus, OB=olfactory bulb, pOB=putative olfactory bulb, SP=subpallium.

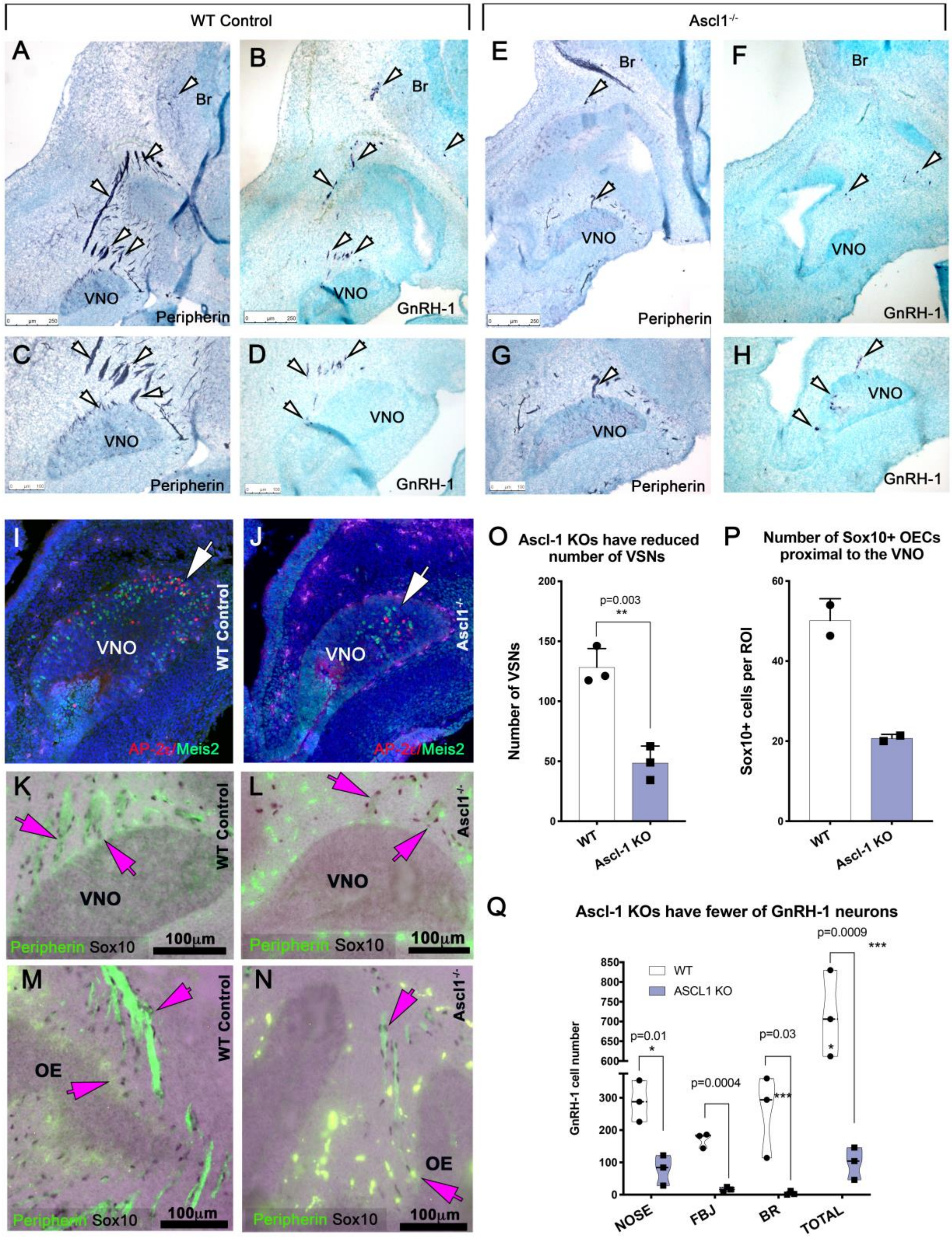
WT Control
Ascl1-/-
A
Br
VNO
Peripherin
B
Br
VNO
GnRH-1
E
Br
VNO
Peripherin
F
Br
VNO
GnRH-1
C
VNO
Peripherin
D
VNO
GnRH-1
G
VNO
Peripherin
H
VNO
GnRH-1
I
VNO
WT Control
AP-2ε/Meis2
J
VNO
Ascl1-/-
AP-2ε/Meis2
K
VNO
WT Control
Peripherin Sox10
100μm
L
VNO
Ascl1-/-
Peripherin Sox10
100μm
M
OE
WT Control
Peripherin Sox10
100μm
N
OE
Ascl1-/-
Peripherin Sox10
100μm
O
Ascl-1 KOs have reduced number of VSNs
p=0.003
**
Number of VSNs
0
50
100
150
200
WT
Ascl-1 KO
P
Number of Sox10+ OECs proximal to the VNO
Sox10+ cells per ROI
0
20
40
60
WT
Ascl-1 KO
Q
Ascl-1 KOs have fewer of GnRH-1 neurons
WT
ASCL1 KO
GnRH-1 cell number
0
100
200
300
600
650
700
750
800
850
p=0.01
*
p=0.0004
p=0.03
***
p=0.0009
***
*
NOSE
FBJ
BR
TOTAL

**Figure 8**. **Ascl-1 KO have a comparable reduction in the number of vomeronasal and GnRH-1 neurons.** A-C) Immunostaining against Peripherin highlights neuronal projections (white arrows) emerging from the VNO of WT animals projecting towards the brain. B,D) In controls, immunostaining against GnRH-1 reveals migratory GnRH-1ns distributed between the VNO and the brain. E,G) In Ascl-1 null mutants, only sparse peripherin positive projections emerge from the OE and VNO (white arrows). F-H) In Ascl-1 KOs, GnRH-1ns emerge from the VNO migrating in the nasal area (white arrows). I,J) AP-2ε and Meis2 immunostaining highlights the reduced number of differentiated VSNs in Ascl-1 KOs (white arrow). K-N) Reduced olfactory and vomeronasal neurons in Ascl-1 KOs does not prevent ensheathing cell formation in the nasal mucosa. K-N) Combined IF anti Peripherin and Sox10 IHC. K,M) In control animals, many Sox10 immunoreactive OECs (magenta arrows) are found around the VNO, along the Peripherin positive vomeronasal bundles, (M) proximal to the developing OE and along the olfactory bundles. Q) In Ascl-1$^{-/-}$ mutants, Sox10 immunoreactive OECs were found associated with the sparse vomeronasal projections (magenta arrows) (N) proximal to the developing OE and along the olfactory bundles (magenta arrows). O-Q) Quantification of VSNs, OECs, and GnRH-1ns in controls and Ascl-1 KOs. Holm-Sidak's multiple comparisons test.

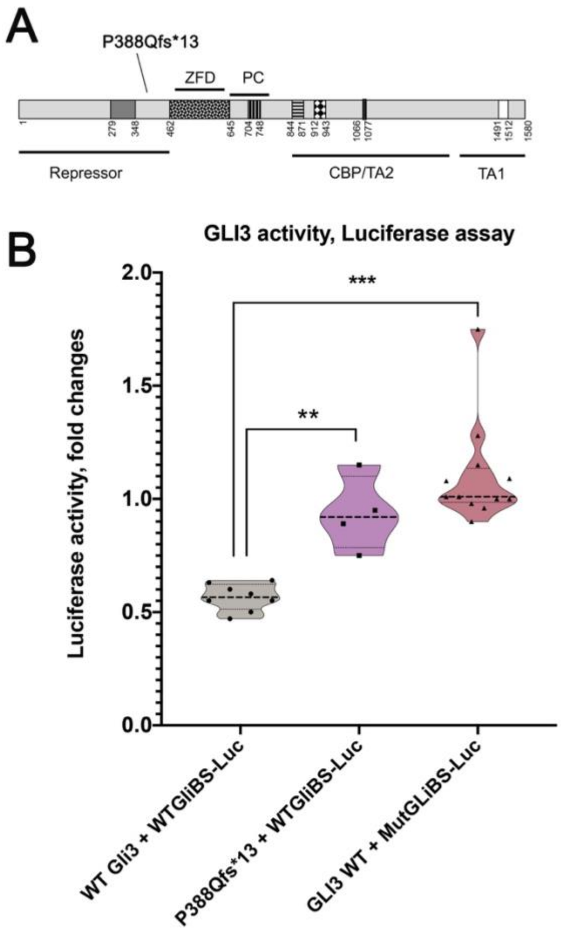

**Fig.9) Functional validation of GLI3 loss-of-function.** Cartoon illustrating *GLI3* protein, the mutation P388Qfs*13 affects the repressor domain of the protein. Zinc finger domain (ZFD), protein cleavage (PC), CBP-binding domain, transactivation domain 1 and 2 (TA1, TA2). B) Luciferase activity assay, the repressor activity of Gli3WT on the reporter (WTGLiBS-Luc) is lost in the truncated GLI3. No repression was found for WT Gli3 on reporter carrying non-functional Gli binding site MutGLiBS-Luc. **p=0.002, ***p<0.0001, Holm-Sidak's multiple comparisons test.

# REFERENCES

1. Miller AM, Treloar HB, and Greer CA. Composition of the migratory mass during development of the olfactory nerve. *J Comp Neurol.* 2010;518(24):4825-41.
2. Casoni F, Malone SA, Belle M, Luzzati F, Collier F, Allet C, et al. Development of the neurons controlling fertility in humans: new insights from 3D imaging and transparent fetal brains. *Development.* 2016;143(21):3969-81.
3. Pingault V, Bodereau V, Baral V, Marcos S, Watanabe Y, Chaoui A, et al. Loss-of-function mutations in SOX10 cause Kallmann syndrome with deafness. *Am J Hum Genet.* 2013;92(5):707-24.
4. Barraud P, St John JA, Stolt CC, Wegner M, and Baker CV. Olfactory ensheathing glia are required for embryonic olfactory axon targeting and the migration of gonadotropin-releasing hormone neurons. *Biol Open.* 2013;2(7):750-9.
5. Taroc EZM, Prasad A, Lin JM, and Forni PE. The terminal nerve plays a prominent role in GnRH-1 neuronal migration independent from proper olfactory and vomeronasal connections to the olfactory bulbs. *Biology open.* 2017;6(10):1552-68.
6. Schwanzel-Fukuda M, and Pfaff DW. Origin of luteinizing hormone-releasing hormone neurons. *Nature.* 1989;338(6211):161-4.
7. Wray S, Grant P, and Gainer H. Evidence that cells expressing luteinizing hormone-releasing hormone mRNA in the mouse are derived from progenitor cells in the olfactory placode. *Proceedings of the National Academy of Sciences of the United States of America.* 1989;86(20):8132-6.
8. Wray S, Nieburgs A, and Elkabes S. Spatiotemporal cell expression of luteinizing hormone-releasing hormone in the prenatal mouse: evidence for an embryonic origin in the olfactory placode. *Brain Res Dev Brain Res.* 1989;46(2):309-18.
9. Forni PE, and Wray S. GnRH, anosmia and hypogonadotropic hypogonadism - Where are we? *Front Neuroendocrinol.* 2015;36C:165-77.
10. Dode C, and Rondard P. PROK2/PROKR2 Signaling and Kallmann Syndrome. *Front Endocrinol (Lausanne).* 2013;4:19.
11. Dode C, Teixeira L, Levilliers J, Fouveaut C, Bouchard P, Kottler ML, et al. Kallmann syndrome: mutations in the genes encoding prokineticin-2 and prokineticin receptor-2. *PLoS genetics.* 2006;2(10):e175.
12. Pablo Mendez J, Zenteno JC, Coronel A, Soriano-Ursua MA, Valencia-Villalvazo EY, Soderlund D, et al. Triallelic digenic mutation in the prokineticin 2 and GNRH receptor genes in two brothers with normosmic congenital hypogonadotropic hypogonadism. *Endocr Res.* 2014:1-6.
13. Pitteloud N, Quinton R, Pearce S, Raivio T, Acierno J, Dwyer A, et al. Digenic mutations account for variable phenotypes in idiopathic hypogonadotropic hypogonadism. *J Clin Invest.* 2007;117(2):457-63.
14. Quaynor SD, Kim HG, Cappello EM, Williams T, Chorich LP, Bick DP, et al. The prevalence of digenic mutations in patients with normosmic hypogonadotropic hypogonadism and Kallmann syndrome. *Fertil Steril.* 2011;96(6):1424-30 e6.

15. Hu D, and Helms JA. The role of sonic hedgehog in normal and abnormal craniofacial morphogenesis. *Development.* 1999;126(21):4873-84.
16. Xavier GM, Seppala M, Barrell W, Birjandi AA, Geoghegan F, and Cobourne MT. Hedgehog receptor function during craniofacial development. *Dev Biol.* 2016;415(2):198-215.
17. Hasenpusch-Theil K, West S, Kelman A, Kozic Z, Horrocks S, McMahon AP, et al. Gli3 controls the onset of cortical neurogenesis by regulating the radial glial cell cycle through Cdk6 expression. *Development.* 2018;145(17).
18. Sasaki H, Nishizaki Y, Hui C, Nakafuku M, and Kondoh H. Regulation of Gli2 and Gli3 activities by an amino-terminal repression domain: implication of Gli2 and Gli3 as primary mediators of Shh signaling. *Development.* 1999;126(17):3915-24.
19. Niewiadomski P, Kong JH, Ahrends R, Ma Y, Humke EW, Khan S, et al. Gli protein activity is controlled by multisite phosphorylation in vertebrate Hedgehog signaling. *Cell Rep.* 2014;6(1):168-81.
20. Pan A, Chang L, Nguyen A, and James AW. A review of hedgehog signaling in cranial bone development. *Front Physiol.* 2013;4:61.
21. Magnani D, Hasenpusch-Theil K, Benadiba C, Yu T, Basson MA, Price DJ, et al. Gli3 controls corpus callosum formation by positioning midline guideposts during telencephalic patterning. *Cereb Cortex.* 2014;24(1):186-98.
22. Magnani D, Hasenpusch-Theil K, Jacobs EC, Campagnoni AT, Price DJ, and Theil T. The Gli3 hypomorphic mutation Pdn causes selective impairment in the growth, patterning, and axon guidance capability of the lateral ganglionic eminence. *J Neurosci.* 2010;30(41):13883-94.
23. Yu T, Fotaki V, Mason JO, and Price DJ. Analysis of early ventral telencephalic defects in mice lacking functional Gli3 protein. *J Comp Neurol.* 2009;512(5):613-27.
24. Fotaki V, Price DJ, and Mason JO. Wnt/beta-catenin signaling is disrupted in the extra-toes (Gli3(Xt/Xt) ) mutant from early stages of forebrain development, concomitant with anterior neural plate patterning defects. *J Comp Neurol.* 2011;519(9):1640-57.
25. Fotaki V, Yu T, Zaki PA, Mason JO, and Price DJ. Abnormal positioning of diencephalic cell types in neocortical tissue in the dorsal telencephalon of mice lacking functional Gli3. *J Neurosci.* 2006;26(36):9282-92.
26. Johnston JJ, Sapp JC, Turner JT, Amor D, Aftimos S, Aleck KA, et al. Molecular analysis expands the spectrum of phenotypes associated with GLI3 mutations. *Hum Mutat.* 2010;31(10):1142-54.
27. Metz H, and Wray S. Use of mutant mouse lines to investigate origin of gonadotropin-releasing hormone-1 neurons: lineage independent of the adenohypophysis. *Endocrinology.* 2010;151(2):766-73.
28. Keino H, Masaki S, Kawarada Y, and Naruse I. Apoptotic degeneration in the arhinencephalic brain of the mouse mutant Pdn/Pdn. *Brain Res Dev Brain Res.* 1994;78(2):161-8.
29. Balmer CW, and LaMantia AS. Loss of Gli3 and Shh function disrupts olfactory axon trajectories. *The Journal of comparative neurology.* 2004;472(3):292-307.

30. Besse L, Neti M, Anselme I, Gerhardt C, Ruther U, Laclef C, et al. Primary cilia control telencephalic patterning and morphogenesis via Gli3 proteolytic processing. *Development.* 2011;138(10):2079-88.
31. Vaaralahti K, Raivio T, Koivu R, Valanne L, Laitinen EM, and Tommiska J. Genetic Overlap between Holoprosencephaly and Kallmann Syndrome. *Mol Syndromol.* 2012;3(1):1-5.
32. Quaynor SD, Bosley ME, Duckworth CG, Porter KR, Kim SH, Kim HG, et al. Targeted next generation sequencing approach identifies eighteen new candidate genes in normosmic hypogonadotropic hypogonadism and Kallmann syndrome. *Molecular and cellular endocrinology.* 2016;437:86-96.
33. Kuschel S, Ruther U, and Theil T. A disrupted balance between Bmp/Wnt and Fgf signaling underlies the ventralization of the Gli3 mutant telencephalon. *Dev Biol.* 2003;260(2):484-95.
34. Matera I, Watkins-Chow DE, Loftus SK, Hou L, Incao A, Silver DL, et al. A sensitized mutagenesis screen identifies Gli3 as a modifier of Sox10 neurocristopathy. *Hum Mol Genet.* 2008;17(14):2118-31.
35. Engelen E, Akinci U, Bryne JC, Hou J, Gontan C, Moen M, et al. Sox2 cooperates with Chd7 to regulate genes that are mutated in human syndromes. *Nat Genet.* 2011;43(6):607-11.
36. Kim YJ, Osborn DP, Lee JY, Araki M, Araki K, Mohun T, et al. WDR11-mediated Hedgehog signalling defects underlie a new ciliopathy related to Kallmann syndrome. *EMBO Rep.* 2018;19(2):269-89.
37. Forni PE, Bharti K, Flannery EM, Shimogori T, and Wray S. The indirect role of fibroblast growth factor-8 in defining neurogenic niches of the olfactory/GnRH systems. *J Neurosci.* 2013;33(50):19620-34.
38. Forni PE, Fornaro M, Guenette S, and Wray S. A role for FE65 in controlling GnRH-1 neurogenesis. *J Neurosci.* 2011;31(2):480-91.
39. Cau E, Gradwohl G, Casarosa S, Kageyama R, and Guillemot F. Hes genes regulate sequential stages of neurogenesis in the olfactory epithelium. *Development.* 2000;127(11):2323-32.
40. Cuschieri A, and Bannister LH. The development of the olfactory mucosa in the mouse: light microscopy. *J Anat.* 1975;119(Pt 2):277-86.
41. Wang H, Ge G, Uchida Y, Luu B, and Ahn S. Gli3 is required for maintenance and fate specification of cortical progenitors. *J Neurosci.* 2011;31(17):6440-8.
42. Lin JM, Taroc EZM, Frias JA, Prasad A, Catizone AN, Sammons MA, et al. The transcription factor Tfap2e/AP-2epsilon plays a pivotal role in maintaining the identity of basal vomeronasal sensory neurons. *Dev Biol.* 2018.
43. Lin JM, Taroc EZM, Frias JA, Prasad A, Catizone AN, Sammons MA, et al. The transcription factor Tfap2e/AP-2ε plays a pivotal role in maintaining the identity of basal vomeronasal sensory neurons. *bioRxiv.* 2018.
44. Enomoto T, Ohmoto M, Iwata T, Uno A, Saitou M, Yamaguchi T, et al. Bcl11b/Ctip2 controls the differentiation of vomeronasal sensory neurons in mice. *J Neurosci.* 2011;31(28):10159-73.
45. Cariboni A, Davidson K, Rakic S, Maggi R, Parnavelas JG, and Ruhrberg C. Defective gonadotropin-releasing hormone neuron migration in mice lacking SEMA3A signalling

through NRP1 and NRP2: implications for the aetiology of hypogonadotropic hypogonadism. *Hum Mol Genet.* 2011;20(2):336-44.

46. Giacobini P, and Prevot V. Semaphorins in the development, homeostasis and disease of hormone systems. *Semin Cell Dev Biol.* 2013;24(3):190-8.

47. Hanchate NK, Giacobini P, Lhuillier P, Parkash J, Espy C, Fouveaut C, et al. SEMA3A, a gene involved in axonal pathfinding, is mutated in patients with Kallmann syndrome. *PLoS genetics.* 2012;8(8):e1002896.

48. Prince JE, Cho JH, Dumontier E, Andrews W, Cutforth T, Tessier-Lavigne M, et al. Robo-2 controls the segregation of a portion of basal vomeronasal sensory neuron axons to the posterior region of the accessory olfactory bulb. *J Neurosci.* 2009;29(45):14211-22.

49. Forni PE, Taylor-Burds C, Melvin VS, Williams T, and Wray S. Neural crest and ectodermal cells intermix in the nasal placode to give rise to GnRH-1 neurons, sensory neurons, and olfactory ensheathing cells. *J Neurosci.* 2011;31(18):6915-27.

50. Rich CA, Perera SN, Andratschke J, Stolt CC, Buehler DP, Southard-Smith EM, et al. Olfactory ensheathing cells abutting the embryonic olfactory bulb express Frzb, whose deletion disrupts olfactory axon targeting. *Glia.* 2018;66(12):2617-31.

51. Naruse I, Fukui Y, Keino H, and Taniguchi M. The arrest of luteinizing hormone-releasing hormone neuronal migration in the genetic arhinencephalic mouse embryo (Pdn/Pdn). *Brain research Developmental brain research.* 1994;81(2):178-84.

52. Veistinen L, Takatalo M, Tanimoto Y, Kesper DA, Vortkamp A, and Rice DP. Loss-of-Function of Gli3 in Mice Causes Abnormal Frontal Bone Morphology and Premature Synostosis of the Interfrontal Suture. *Front Physiol.* 2012;3:121.

53. Aoto K, Nishimura T, Eto K, and Motoyama J. Mouse GLI3 regulates Fgf8 expression and apoptosis in the developing neural tube, face, and limb bud. *Developmental biology.* 2002;251(2):320-32.

54. Blaess S, Stephen D, and Joyner AL. Gli3 coordinates three-dimensional patterning and growth of the tectum and cerebellum by integrating Shh and Fgf8 signaling. *Development.* 2008;135(12):2093-103.

55. Anderson SA, Eisenstat DD, Shi L, and Rubenstein JL. Interneuron migration from basal forebrain to neocortex: dependence on Dlx genes. *Science.* 1997;278(5337):474-6.

56. Lavdas AA, Grigoriou M, Pachnis V, and Parnavelas JG. The medial ganglionic eminence gives rise to a population of early neurons in the developing cerebral cortex. *J Neurosci.* 1999;19(18):7881-8.

57. Wichterle H, Garcia-Verdugo JM, Herrera DG, and Alvarez-Buylla A. Young neurons from medial ganglionic eminence disperse in adult and embryonic brain. *Nat Neurosci.* 1999;2(5):461-6.

58. Wichterle H, Turnbull DH, Nery S, Fishell G, and Alvarez-Buylla A. In utero fate mapping reveals distinct migratory pathways and fates of neurons born in the mammalian basal forebrain. *Development.* 2001;128(19):3759-71.

59. Markram H, Toledo-Rodriguez M, Wang Y, Gupta A, Silberberg G, and Wu C. Interneurons of the neocortical inhibitory system. *Nat Rev Neurosci.* 2004;5(10):793-807.

60. Feng W, Simoes-de-Souza F, Finger TE, Restrepo D, and Williams T. Disorganized olfactory bulb lamination in mice deficient for transcription factor AP-2epsilon. *Mol Cell Neurosci.* 2009;42(3):161-71.

61. Kramer PR, and Wray S. Midline nasal tissue influences nestin expression in nasal-placode-derived luteinizing hormone-releasing hormone neurons during development. *Dev Biol.* 2000;227(2):343-57.

62. Miller SR, Benito C, Mirsky R, Jessen KR, and Baker CVH. Neural crest Notch/Rbpj signaling regulates olfactory gliogenesis and neuronal migration. *Genesis.* 2018;56(6-7):e23215.

63. Sasaki H, Hui C, Nakafuku M, and Kondoh H. A binding site for Gli proteins is essential for HNF-3beta floor plate enhancer activity in transgenics and can respond to Shh in vitro. *Development.* 1997;124(7):1313-22.

64. Saitsu H, Komada M, Suzuki M, Nakayama R, Motoyama J, Shiota K, et al. Expression of the mouse Fgf15 gene is directly initiated by Sonic hedgehog signaling in the diencephalon and midbrain. *Dev Dyn.* 2005;232(2):282-92.

65. Krauss S, Foerster J, Schneider R, and Schweiger S. Protein phosphatase 2A and rapamycin regulate the nuclear localization and activity of the transcription factor GLI3. *Cancer Res.* 2008;68(12):4658-65.

66. Young J, Metay C, Bouligand J, Tou B, Francou B, Maione L, et al. SEMA3A deletion in a family with Kallmann syndrome validates the role of semaphorin 3A in human puberty and olfactory system development. *Hum Reprod.* 2012;27(5):1460-5.

67. Ohtsuka T, Sakamoto M, Guillemot F, and Kageyama R. Roles of the basic helix-loop-helix genes Hes1 and Hes5 in expansion of neural stem cells of the developing brain. *J Biol Chem.* 2001;276(32):30467-74.

68. Ohtsuka T, Ishibashi M, Gradwohl G, Nakanishi S, Guillemot F, and Kageyama R. Hes1 and Hes5 as notch effectors in mammalian neuronal differentiation. *EMBO J.* 1999;18(8):2196-207.

69. Lange C, Huttner WB, and Calegari F. Cdk4/cyclinD1 overexpression in neural stem cells shortens G1, delays neurogenesis, and promotes the generation and expansion of basal progenitors. *Cell Stem Cell.* 2009;5(3):320-31.

70. Pilaz LJ, Patti D, Marcy G, Ollier E, Pfister S, Douglas RJ, et al. Forced G1-phase reduction alters mode of division, neuron number, and laminar phenotype in the cerebral cortex. *Proc Natl Acad Sci U S A.* 2009;106(51):21924-9.

71. Miller SR, Perera SN, Benito C, Stott SR, and Baker CV. Evidence for a Notch1-mediated transition during olfactory ensheathing cell development. *J Anat.* 2016;229(3):369-83.

72. Barraud P, Seferiadis AA, Tyson LD, Zwart MF, Szabo-Rogers HL, Ruhrberg C, et al. Neural crest origin of olfactory ensheathing glia. *Proc Natl Acad Sci U S A.* 2010;107(49):21040-5.

73. Geller S, Kolasa E, Tillet Y, Duittoz A, and Vaudin P. Olfactory ensheathing cells form the microenvironment of migrating GnRH-1 neurons during mouse development. *Glia.* 2013;61(4):550-66.

74. Richter MW, Fletcher PA, Liu J, Tetzlaff W, and Roskams AJ. Lamina propria and olfactory bulb ensheathing cells exhibit differential integration and migration and promote

differential axon sprouting in the lesioned spinal cord. *J Neurosci.* 2005;25(46):10700-11.

75. Ito D, Ibanez C, Ogawa H, Franklin RJ, and Jeffery ND. Comparison of cell populations derived from canine olfactory bulb and olfactory mucosal cultures. *Am J Vet Res.* 2006;67(6):1050-6.

76. Mayeur A, Duclos C, Honore A, Gauberti M, Drouot L, do Rego JC, et al. Potential of olfactory ensheathing cells from different sources for spinal cord repair. *PLoS One.* 2013;8(4):e62860.

77. Al-Qattan MM, Shamseldin HE, Salih MA, and Alkuraya FS. GLI3-related polydactyly: a review. *Clin Genet.* 2017;92(5):457-66.

78. Kroisel PM, Petek E, and Wagner K. Phenotype of five patients with Greig syndrome and microdeletion of 7p13. *Am J Med Genet.* 2001;102(3):243-9.

79. Sykiotis GP, Plummer L, Hughes VA, Au M, Durrani S, Nayak-Young S, et al. Oligogenic basis of isolated gonadotropin-releasing hormone deficiency. *Proceedings of the National Academy of Sciences of the United States of America.* 2010;107(34):15140-4.

80. Leanos-Miranda A, Ulloa-Aguirre A, Janovick JA, and Conn PM. In vitro coexpression and pharmacological rescue of mutant gonadotropin-releasing hormone receptors causing hypogonadotropic hypogonadism in humans expressing compound heterozygous alleles. *J Clin Endocrinol Metab.* 2005;90(5):3001-8.

81. Gianetti E, Hall JE, Au MG, Kaiser UB, Quinton R, Stewart JA, et al. When Genetic Load Does Not Correlate with Phenotypic Spectrum: Lessons from the GnRH Receptor (GNRHR). *The Journal of clinical endocrinology and metabolism.* 2012;97(9):E1798-807.

82. Schimmang T, Lemaistre M, Vortkamp A, and Ruther U. Expression of the zinc finger gene Gli3 is affected in the morphogenetic mouse mutant extra-toes (Xt). *Development.* 1992;116(3):799-804.

83. Kim EJ, Ables JL, Dickel LK, Eisch AJ, and Johnson JE. Ascl1 (Mash1) defines cells with long-term neurogenic potential in subgranular and subventricular zones in adult mouse brain. *PLoS One.* 2011;6(3):e18472.

84. Kagoshima M, and Ito T. Diverse gene expression and function of semaphorins in developing lung: positive and negative regulatory roles of semaphorins in lung branching morphogenesis. *Genes Cells.* 2001;6(6):559-71.

85. Kinzler KW, Ruppert JM, Bigner SH, and Vogelstein B. The GLI gene is a member of the Kruppel family of zinc finger proteins. *Nature.* 1988;332(6162):371-4.

86. Balasubramanian R, and Crowley WF, Jr. Isolated GnRH deficiency: a disease model serving as a unique prism into the systems biology of the GnRH neuronal network. *Mol Cell Endocrinol.* 2011;346(1-2):4-12.

87. Doty RL. Office procedures for quantitative assessment of olfactory function. *Am J Rhinol.* 2007;21(4):460-73.

88. Lewkowitz-Shpuntoff HM, Hughes VA, Plummer L, Au MG, Doty RL, Seminara SB, et al. Olfactory phenotypic spectrum in idiopathic hypogonadotropic hypogonadism: pathophysiological and genetic implications. *J Clin Endocrinol Metab.*97(1):E136-44.

89. Guo MH, Plummer L, Chan YM, Hirschhorn JN, and Lippincott MF. Burden Testing of Rare Variants Identified through Exome Sequencing via Publicly Available Control Data. *Am J Hum Genet.* 2018;103(4):522-34.

90. Karczewski KJ, Francioli LC, Tiao G, Cummings BB, Alföldi J, Wang Q, et al. Variation across 141,456 human exomes and genomes reveals the spectrum of loss-of-function intolerance across human protein-coding genes. *bioRxiv.* 2019:531210.

E11.5
E13.5
E15.5
GnRH-1
A
NA
Br
OE
VNO
B
OB
Br
NA
POA
VNO
C
OB
Br
NA
VNO
A1
OE
VNO
B1
VNO
C1
VNO
Gli3
D
OE
RE
VNO
E
VNO
F
VNO
PHH3
G
OE
RE
VNO
H
VNO
I
VNO
Ascl-1
J
0 µm 50
K
0 µm 100
L
100 µm 0
AP-2ε
M
RE
OE
VNO
N
VNO
O
VNO
Meis2
P
RE
OE
VNO
Q
VNO
R
VNO

A
Hes-1
0 µm 100
B
Hes-1
0 µm 50
C
Ascl-1
D
Ascl-1
E
Gli3
F
Gli3
G
Hes-1Gli3
H
Hes-1Gli3
I
Basal
Gli3
Ascl-1
HES-1
Apical
Ascl-1+ Neuro-progenitor cells
VSNs
Hes1+ Neuroepithelial Stem Cells

A
E15.0 WT Control
VNO
Meis2/AP-2ε
B
E15.0 Gli3Xt/Xt
VNO
Meis2/AP-2ε
C
Number of VSNs
Cells/section
400
300
200
100
0
Control
Gli3Xt/WT
Gli3Xt/Xt
p=0.02
*
n.s.
n.s.
p=0.03
*
n.s.
n.s.
p=0.03
*
n.s.
n.s.
AP-2ε+ VSNs
Meis2+ VSNs
Total VSNs
E
E15.0 WT Control
basal
apical
PHH3
F
E15.0 Gli3Xt/Xt
basal
apical
PHH3
D
Number of deviding progenitors
number of deviding cells/section
80
60
40
20
0
WT
Gli3Xt/WT
Gli3Xt/Xt
*p=0.01
*p=0.03
**p=0.001
PHH3+ Basal
PHH3+ Apical
Total PHH3+ cells
H
E15.0 WT Control
Ascl-1
0 µm 100
I
E15.0 Gli3Xt/Xt
Ascl-1
0 µm 100
E
Number of Ascl-1+ cells
number of ASCL1 + cells/section
250
200
150
100
50
0
* p=0.025
Control
Gli3Xt/WT
Gli3Xt/Xt

A
Ctx
OB
SP
FBJ
NA
Hyp
WT E15
GnRH-1
B
SP
NA
VNO
$Gli3^{Xt/Xt}$ E15
GnRH-1
250µm
C
VNO
100µm
GnRH-1
D
100µm
GnRH-1
E
OE
VNO
GnRH-1
100µm
F
GnRH-1
100µm
G
Ctx
OB
FBJ
SP
GnRH-1
H
SP
OE
GnRH-1
E15.5 GnRH-1 migration in $Gli3^{XT}$ mutants
I
Number of GnRH-1 neurons
1500
1000
500
0
p=0.0008
***
p=0.0081
**
p=0.012
*
p=0.02
*
n.s.
p=0.000005
****
p=0.04
*
p=0.00009
***
n.s.
WT
$Gli3^{xt/Wt}$
$Gli3^{Xt/Xt}$
Nasal area
Forebrain junction
Forebrain
Total

E15.0 WT Control
E15.0 Gli3Xt/Xt
A
OB
AOB
TN
VSNs
OSNs
FB
E15.0 WT Control
GnRH-1 Peripherin
B
TN
FB
FCM
(OSNs/VSNs)
E15.0 Gli3Xt/Xt
GnRH-1 Peripherin
C
AOB
TN
MOB
bFB
OSNs
VSNs
Peripherin
D
TN
TN
OSNs
VSNs
Peripherin
E
AOB
TN
MOB
bFB
OSNs
VSNs
Robo2
F
TN
TN
OSNs
VSNs
Robo2
G
AOB
TN
MOB
bFB
OSNs
VSNs
Nrp2
H
TN
TN
OSNs
VSNs
Nrp2
I
AOB
TN
MOB
bFB
OSNs
VSNs
Peripherin/Nrp2/Robo2
J
TN
OSNs
VSNs
Peripherin/Nrp2/Robo2
K
Nrp2
Robo2
Nrp1
L
Nrp1
Nrp2
Robo2
K1
TN
Br
Peripherin
L1
TN
Peripherin
K2
TN
Br
Nrp1
L2
TN
Nrp1
E15.0 WT Control
E15.0 Gli3Xt/Xt
M
Peripherin/GnRH-1
N
Peripherin/GnRH-1
M1
VSNs
VNO
Peripherin
M2
Robo2
N1
pTN
VSNs
pTN
VNO
Peripherin
N2
Nrp2
M3
Nrp2
M4
Peripherin/Nrp2/Robo2
N3
Robo2
N4
Peripherin/Nrp2/Robo2
O1
Peripherin
O2
Nrp1
O3
GnRH-1
O4
GnRH1 Nrp1 Peripherin
P
OB
Br
MM
Sox10
OE
VNO
TG
Q
Br
Sox10
MM
OE
VNO
TG
R
Peripherin Sox10
VNO
100μm
S
Peripherin Sox10
VNO
100μm
T
Number of Sox10+ OECs proximal to the VNO
Sox10+ cells /334.500μm² field
80
60
40
20
0
****
****
****
Control
Gli3Xt/WT
Gli3Xt/Xt

A
WT 5mo
500µm
GnRH-1
B
Gli3$^{Xt/WT}$ Het 5mo
500µm
GnRH-1
C
Total GnRH 5mo Male Brain
n.s.
# Cells
1500
1000
500
0
WT
Gli3$^{XT/WT}$
D
OD of GnRH in Median Eminence
n.s.
OD
0.20
0.15
0.10
0.05
0.00
WT
Gli3$^{XT/WT}$
E
WT 5mo
200µm
3V
ME
GnRH-1
F
Gli3$^{Xt/WT}$ Het 5mo
200µm
3V
ME
GnRH-1

A
OB
SP
VNO
Control
AP-2ε GAD1
B
SP
pOB
VNO
Gli3 Xt/Xt
AP-2ε GAD1
C
OB
SP
AP-2ε GAD1
100µm
D
pOB
AP-2ε GAD1
100µm
E
Ctx
OB
Ac
SP
Hyp
F
Ctx
SP
OB
Hyp
G
Ctx
Control
OB
Sema3A
H
Ctx
Gli3 Xt/Xt
Sema3A

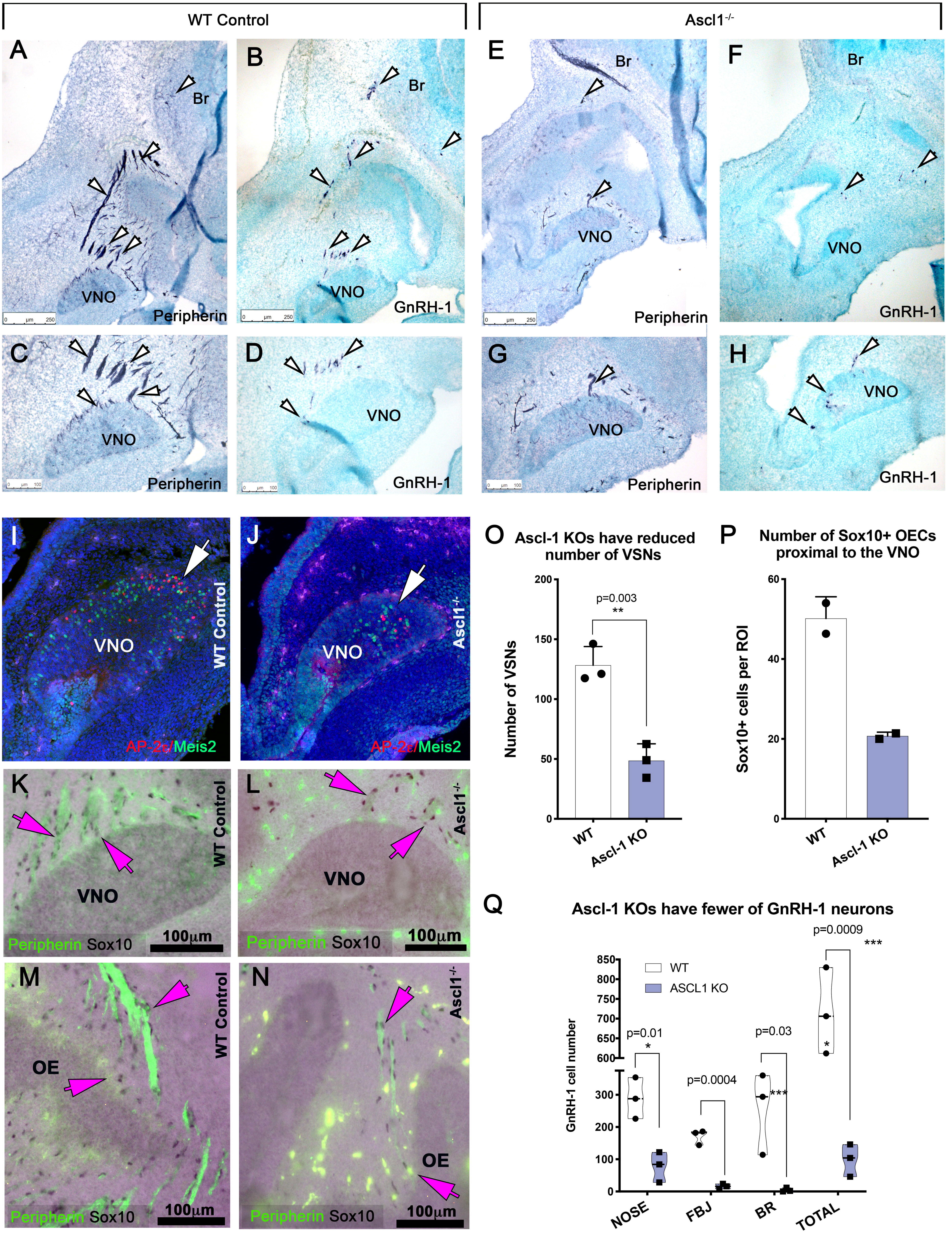
WT Control
Ascl1-/-
A
Br
VNO
Peripherin
0 µm 250
B
Br
VNO
GnRH-1
0 µm 250
E
Br
VNO
Peripherin
0 µm 250
F
Br
VNO
GnRH-1
C
VNO
Peripherin
0 µm 100
D
VNO
GnRH-1
0 µm 100
G
VNO
Peripherin
0 µm 100
H
VNO
GnRH-1
I
VNO
WT Control
AP-2ε/Meis2
J
VNO
Ascl1-/-
AP-2ε/Meis2
K
VNO
WT Control
Peripherin Sox10
100µm
L
VNO
Ascl1-/-
Peripherin Sox10
100µm
M
OE
WT Control
Peripherin Sox10
100µm
N
OE
Ascl1-/-
Peripherin Sox10
100µm
O
Ascl-1 KOs have reduced number of VSNs
Number of VSNs
0
50
100
150
200
p=0.003
**
WT
Ascl-1 KO
P
Number of Sox10+ OECs proximal to the VNO
Sox10+ cells per ROI
0
20
40
60
WT
Ascl-1 KO
Q
Ascl-1 KOs have fewer of GnRH-1 neurons
GnRH-1 cell number
0
100
200
300
600
650
700
750
800
850
WT
ASCL1 KO
p=0.01
*
p=0.0004
p=0.03
***
p=0.0009
***
*
NOSE
FBJ
BR
TOTAL

A
P388Qfs*13
ZFD
PC
1
279
348
462
645
704
748
844
871
912
943
1066
1077
1491
1512
1580
Repressor
CBP/TA2
TA1
B
GLI3 activity, Luciferase assay
Luciferase activity, fold changes
0.0
0.5
1.0
1.5
2.0
***
**
WT Gli3 + WTGliBS-Luc
P388Qfs*13 + WTGliBS-Luc
GLI3 WT + MutGLiBS-Luc